Steady-State Continuous-Flow Purification by Free-Flow Electrophoresis

Fletcher John Agostino

A DISSERTATION SUBMITTED TO
THE FACULTY OF GRADUATE STUDIES
IN PARTIAL FULFILLMENT OF THE REQUIREMENTS
FOR THE DEGREE OF
DOCTOR OF PHILOSOPHY

GRADUATE PROGRAM IN CHEMISTRY
YORK UNIVERSITY
TORONTO, ONTARIO

January 2015

Abstract

Synthesis, purification, and analysis are fundamental in chemical processing, and can be achieved by continuous-flow or batch strategies. Continuous-flow technology facilitates chemical syntheses and can improve production efficiency. For product isolation and analysis, continuous-flow systems can be used to facilitate high-throughput purification as well as real-time monitoring. The combination of synthesis, purification, and analysis (in-flow) is a challenging feat due to the scarce number of continuous-flow purification techniques that exist. A potential continuous-flow purification candidate to integrate with continuous-flow chemistry is Free-Flow Electrophoresis (FFE). FFE devices are available at the macro-scale, milli-scale (mFFE), and micro-scale (μFFE). In FFE, samples are carried by a pressure-driven hydrodynamic flow through a high aspect ratio channel, in which a voltage is applied perpendicular to the flow. The electric field forces the individual components of the sample to separate based on differences in their charge-to-size ratios, also called electrophoretic mobilities. Separation, however, can be easily compromised by the generated electric current. Typical currents in FFE result in Joule heating and electrolysis; which produces bubbles along with by-products that can alter pH. Over time, steady-state purification is compromised and can rapidly deteriorate separation quality. Macro-scale FFE devices are capable of overcoming issues that destroy steady-state purification; however, their implemented strategies are not easily transferrable to small-scale devices (mFFE and μFFE). Both mFFE and μFFE devices are attractive purification techniques because they use less reagent and sample material than macro-scale FFE, and have already been combined with real-time continuous-flow analysis. Therefore, establishing steady-state continuous-flow purification in small-scale devices can have significant advantages for streamlining, especially continuous-flow synthesis. In this dissertation, I introduce novel geometric modifications that ultimately provide steady-state purification over a wide range of mFFE separation conditions. These modifications include i) chimneys, which are used to evacuate bubbles completely from mFFE devices, and ii) sacrificial channels, which maintain flow uniformity and reduce pH gradients. Both chimney and sacrificial channel geometries were thoroughly optimized to allow consistent separation

conditions over long periods of time. The combination of chimneys and sacrificial channels allows at least 12 hours of continuous-flow purification; thus, facilitating its integration with other continuous-flow techniques.

Dedications

To my Mom and my Dad, who filled my past with unconditional love.

&

To Jennie, my love and my future, who put up with me finishing the last 2 years of my PhD over the past 4 years.

Acknowledgements

First and foremost, I would like to acknowledge my supervisor, Professor Sergey Krylov. As an administrator he has helped me develop a better sense of priorities and planning. As a scientific advisor, he has enabled me to develop scientific ideas into outstanding theories with practical applications. As a mentor, he has inspired me to seek out the answers to the all questions in life (no matter how ridiculous the question).

From our laboratory, I would like to acknowledge several people. Mirzo and Dave, my partners in crime, we have been here together from the start. Without them, this experience would not have been as rewarding. Our long discussions about science, work, home, and life have been thoroughly enjoyed and I have learned so much from both of them. Jiayin, who joined a few months later, many thanks for all the lunches together and our practical attempts to make FFE something special.

To Drs. Michael Musheev, Alex Petrov, Victor Galievsky, Leonid Cherney, and Chris Evenhuis, I have greatly appreciated their significant contributions to my project. They have helped advance my knowledge of COMSOL simulations, physics, mathematics, and chemistry; I hope to always retain their important lessons.

To all Krylov members, past and present, a million thanks for your collaborations and your friendships. We are all fortunate to have met each other and travelled down the same road together, and all of these memories will not be soon forgotten.

To Professors Sylvie Morin and Derek Wilson, they have always been generous with their time, guidance, and insight. Their presence has helped make my scientific contributions more important.

I wish to offer a special thank you to the machine, electronic, and glass shops in Petrie. They allowed me to tap into some personal engineering skills that I did not know existed.

Thanks, as always, to our Canadian funding agencies, and OGS.

TABLE OF CONTENTS

LIST OF TABLES

LIST OF FIGURES

COMMONLY USED ABBREVIATIONS

3D: Three Dimensional

AO: Anode Outlet

CO: Cathode Oulet

CH_2Cl_2: Dichloromethane

CFA: Continuous-Flow Analysis

CFC: Continuous-Flow Chemistry

CFS: Continuous-Flow Synthesis

CFP: Continuous-Flow Purification

E: Electric Field Strength (V/cm)

FFE: Free-Flow Electrophoresis

FFFSE: Free-Flow Field-Step Electrophoresis

FFIZF: Free-Flow Interval Zone Electrophoresis

FFITP: Free-Flow Isotachophoresis

FFIEF: Free-Flow Iso-Electric Focusing

FFZE: Free-Flow Zone Electrophoresis

FR: Feed Rate

mFFE: Milli-FFE

µFFE: Micro-FFE

h: Hour

HEPES: 4-(2-hydroxyethyl)-1-piperazineethanesulfonic acid

MEKC: Micellar ElectroKinetic Chromatography

MS: Mass Spectrometry

min: Minute

NOFFE: Non-Orthogonal-to-the-Flow FFE

PMMA: Poly(methyl methacrylate)

rpm: Revolutions Per Minute

R_s: Resolution

s: Second

SacC: Sacrificial Channel

SacZ: Sacrificial Zone

SC: Separation Channel

SMB: Simulated Moving Bed

SMBC: Simulated Moving Bed Chromatography

SMBR: Simulated Moving Bed Reactors

SZ: Separation Zone

UV: Ultraviolet

CHAPTER 1: INTRODUCTION

1.1 Continuous-Flow Chemistry vs. Batch Chemistry

The essence of continuous-flow chemistry (CFC) is simple: target solutes are propagated by a carrier fluid and processed in an uninterrupted fashion. The opposite of CFC would be batch processing, in which all solutes are combined and processed in a 'one pot' fashion. Since CFC relies heavily on fluid flow rates, it can offer greater control over mixing, and time dependent processes. Such control in a system can maximize efficiency, high-throughput capabilities, and facilitate real-time monitoring. Batch chemistry, on the other hand, is accomplished in a much simpler fashion, which does not permit as much control over experimental conditions. As a result, batch processes are used more as an effective means of testing preliminary experiments for exploratory chemistry. Batch chemistry is prevalent in bench-top experiments, whereas CFC has been intensively used in large-scale industrial manufacturing. An important conclusion that can be extracted from such a basic comparison between CFC and batch chemistry is that a user of CFC will undoubtedly have more control over processing. Regardless of the method, both continuous-flow and batch chemistries can be used successfully to carry out synthesis, purification, and analysis.

With respect to synthesis, purification, and analysis, batch systems carry these out as three individual processes (although analysis is often combined with purification), which can be time consuming and labour intensive. Conceptually, CFC is not restricted by such limitations. To fully exploit the benefits of CFC, it would be ideal to physically connect, in series, chemical synthesis with continuous-flow purification (CFP) and continuous-flow analysis (CFA). Such a tandem combination would permit feedback for automated process control and recycling of unused materials for highly economical operation (**Figure 1.1)**. The introduction of my dissertation will review the present state of continuous-flow synthesis (CFS) and CFP. While CFA is an important aspect of the fully-integrated CFC vision, it is beyond the scope of my research and will be discussed only briefly.

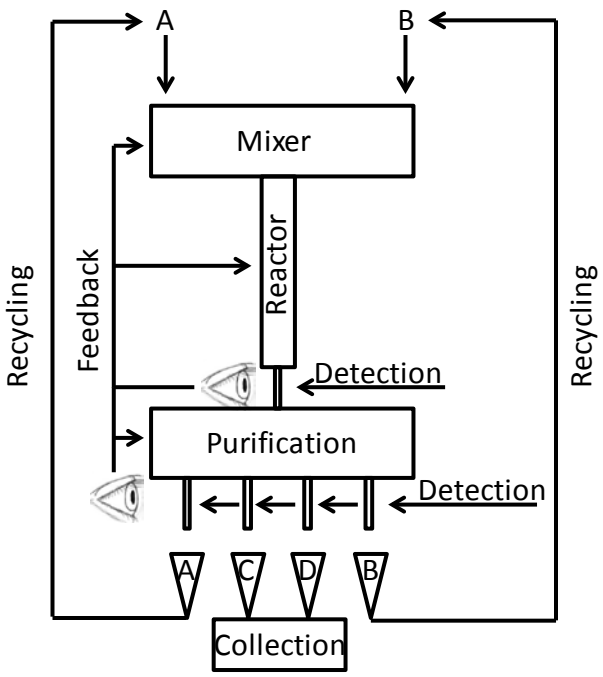

Figure 1.1: A schematic of a fully integrated and interconnected CFC design.

1.2 Large-Scale Continuous-Flow Synthesis

In CFS, chemical reactions are carried out in a fluid stream in a steady-state fashion. CFS takes its roots from successful attempts to streamline 19th century industrial-scale production. In 1864, Ernest Solvay developed a revolutionary technique that continuously produced sodium carbonate by employing the ammonia-soda process. This process, using CFS, allowed for an interconnection of multiple feedback loops, which maximized reaction efficiency and minimized reagent waste. Largely due to this drastic improvement, the production of sodium carbonate increased over an order of magnitude by the turn of the 20th century[2]. The Solvay process, with some modifications, is still in use today.

The benefits of CFS for large-scale production were obvious from the beginning. Large-scale production can be achieved without the need for large-volume reactors, which are difficult to control and often unsafe. The amount of waste generated can be drastically decreased, while the intermediate products

or unreacted starting material can be recycled. The build-up of large amounts of hazardous chemicals can be avoided and hazardous materials can be managed in a streamlined and safe manner. These benefits facilitated decreased production cost and increased production scale. Appreciation of these benefits has led to the use of CFS in many modern large-scale industrial applications. To date, the most abundantly produced chemicals are the raw chemicals that form the majority of starting reagents and solvents in chemical reactions. Raw chemicals are required in large amounts and this demand can be met because they are typically produced by CFS processes, thus, benefitting from high efficiency and low cost. Interestingly, by employing CFS chemical plants serendipitously adopted at least two of the principles of Green Chemistry formulated at the turn of the 21st century: prevention and atom economy[3,4]. The greener nature of CFS can offer important insight into new synthetic strategies and the optimization of pre-existing protocols. In fact, additional Green advantages were realized when small-scale CFS was introduced.

1.3 Small-Scale Continuous-Flow Synthesis

While produced in large abundance, raw chemicals represent only a minor fraction of the variety of all synthesized chemicals. The vast majority of chemicals are fine chemicals produced at small or very small scales, with an emphasis on quality and purity. An ultimate example is the synthesis of highly-diverse combinatorial libraries containing billions of different structures with as few as a thousand copies of every structure[5]. Until recently, batch production of fine chemicals was the only available option. Fine chemical synthetic strategies changed over the last decade when small-scale CFS was developed using capillary and channel micro-reactors. The advantages of small-scale CFS, over a batch approach, include: (i) greater control over the precision of reaction conditions (i.e. temperature, pressure, quality of mixing)[6,7], (ii) ability to use high temperature and pressure[8], (iii) suitability for in-line monitoring of reaction efficiency[9], (iv) automation capabilities[10,11], (v) safer handling of hazardous reactions[12], (vi) and

simple scale-up strategies for larger product quantities[13,14]. The efficiency, versatility, and safety associated with micro-reactors are possible due to rapid mass and heat transport processes. The success of small-scale CFS is attested by the availability of commercial equipment, which has been used for a variety of chemical reactions[15-17]. Overall, the multitude of advantages associated with small-scale CFS has been acknowledged by both the fine-chemicals and pharmaceutical industries, which are beginning to adopt continuous-flow methodologies.

The most significant step towards industrial small-scale CFS will require a concerted effort to integrate inline CFS. To date, however, CFS is typically followed by discontinuous purification. The main reason for the use of discontinuous purification is that a limited number of options for CFP are available. Here, I will discuss all CFP techniques that are viable in-line options to CFS.

1.4 Continuous-Flow Purification Strategies for Continuous-Flow Synthesis

I define continuous-flow strategies as those which process an undivided sample stream that is propagated by an unperturbed flow. The integration of CFP to CFS must satisfy the following criteria. (i) A purification device should resolve target analytes from impurities, by-products, and unused reagents, with minimal contamination. (ii) The purification device should also be compatible with the solvent used in the flow reactor. (iii) Finally, integrating CFS with CFP should not interfere with the steady-state performance of the entire CFC design. Until recently, difficulties in satisfying these criteria have precluded the integration of CFP into CFC designs. To date, there exist only four purification platforms that can be considered as potentially viable with CFC: simulated moving bed chromatography (SMBC); liquid-liquid extraction, magnetophoresis, and electrophoresis. In this section, I review them.

1.4.1 Simulated Moving Bed Chromatography

SMBC, like column chromatography, purifies a sample by adsorption/desorption events between an eluent and a resin, also called the mobile and stationary phase, respectively. The components are separated based on their unique affinities to each phase. In column chromatography a discrete volume of sample is purified, and the next sample does not get injected until separation of the first sample has completed. SMBC achieves purification by injecting discrete volumes of a sample over multiple columns that are connected in series. As the components of a sample are resolved they are collected by the appropriate output valve. The component that remains in the mobile phase is called the extract and the component that is strongly adsorbed to the resin called the raffinate. Both the extract and the raffinate are transported by the eluent. A schematic of a SMBC setup is illustrated in **Figure 1.2**. The columns are stationary, but the valves that control feed, eluent, desorbent, and raffinate rotate in position. In this fashion a sample is allowed to be injected and extracted by an automated valve switch. The sample itself is purified in individual columns, in the same fashion as column chromatography. Combining automatic rotating switches with column chromatography simulates a continuous-flow of sample purification.

Successful implementation of SMBC requires a number of assumptions: constant fluid velocity throughout the system; all columns have identical void fractions; the system maintains isothermal conditions; and no radial concentration gradients in the column[18]. The stringency associated with these requirements suggests that a great deal of optimization is necessary for purification. Maximizing the efficiency and the 'continuous' movement of a sample is achieved when a SMBC setup consists of a large number of columns and the valve switching occurs at high frequencies. In general, SMBC is ideal for the separation of a binary sample. Realistically, however, most sample purification does not involve the separation of two components. SMBC has recently been applied to multicomponent sample and requires a great deal more optimization, enrichment stages[19], cascading SMBC columns[20], and significant valve coordination.

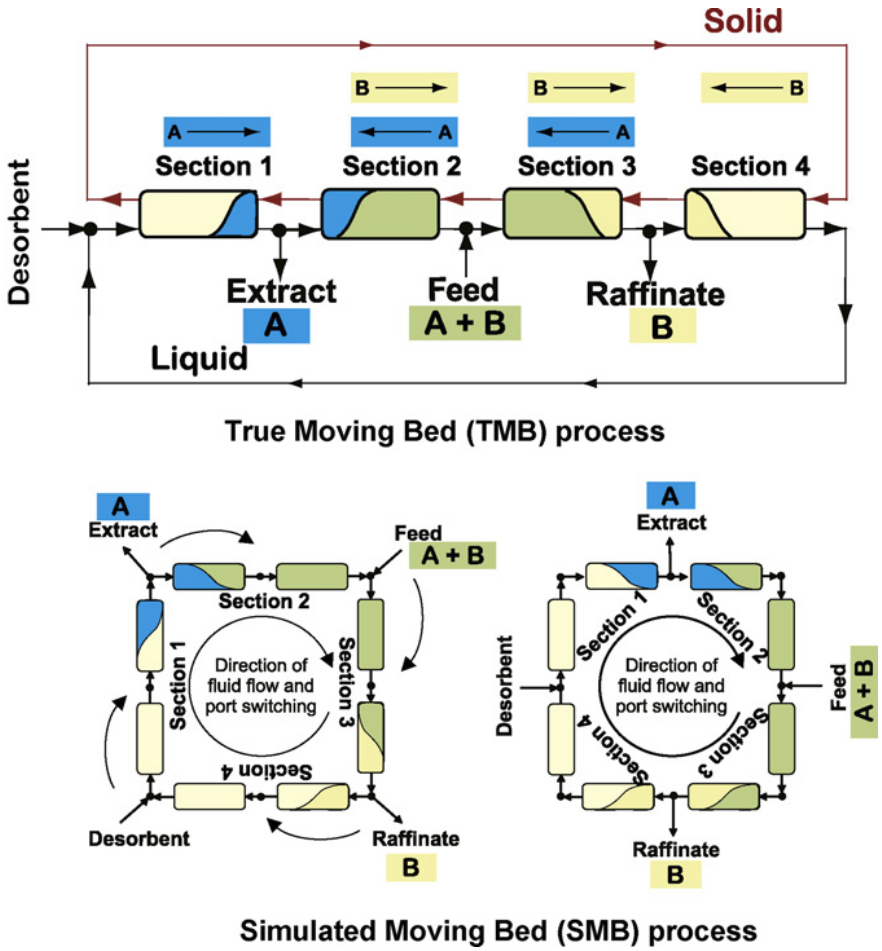

Figure 1.2: Schematic of four-section true moving bed (TMB) and simulated moving bed (SMB) units separating a binary mixture (A and B). The arrows in the TMB scheme indicate the direction of the species fluxes in each section of the unit working under complete separation conditions. The dashed arrows in the SMB scheme represent the port switch. Reproduced from **Ref 18**, with permission, from Elsevier.

The need for purifying multicomponent systems helped create a new field, which was inspired by SMB technology, called simulated moving bed reactors (SMBR). SMBR combines synthesis and purification, in one step, for dissociation reactions (A → B + C). Although SMBR becomes limited to one type of reaction, this synthesis is common among bio-reactors which process enzymatic reactions[21]. SMB technology is highly valuable as these types of separations have been established for decades.

As an important side note: for the sake of the definition of continuous-flow strategies (**Section 1.4**) and the scope of this dissertation, it is difficult to consider SMBC as a *purely* continuous-flow technique. Automation and robotic handling achieve continuous processing of discrete volumes and, thus,

the original fluid stream is divided into smaller volumes. Nevertheless, SMBC deserves to be mentioned as it has already been implemented and commercialized extensively.

1.4.2 Liquid-Liquid Extraction

Liquid-liquid extraction is a purification technique that is based on the separation of non-miscible liquids. Conceivably, target solutes can also be extracted and isolated based on their solubility within a specific liquid phase[22-24]. Extraction efficiency depends on the difference in polarity of each liquid phase and the solubility of the target solute within each phase. Membranes are not necessary but, in some cases, can help to maximize separation efficiency. Classically performed in batch, liquid-liquid extraction procedures have been developed for continuous processing.

A proof of principle continuous-flow extraction unit, with an integrated membrane, was developed by Kralj et al.[25]. In their work, two non-miscible liquids were continuously combined in a slug-flow microreactor and then separated by an in-line extraction unit. The principles of extraction are the following: the extraction unit is divided in two halves by a porous Teflon membrane, allowing only the organic phase to pass to the opposite side of the membrane (**Figure 1.3**). Organic phase transfer is

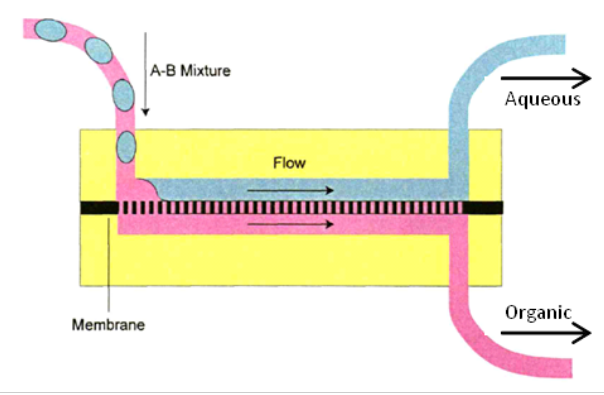

Figure 1.3: A schematic depiction of continuous liquid-liquid extraction. A segmented flow of an aqueous solution (**A**) dispersed in an organic phase (**B**). The organic phase wets the hydrophobic membrane and is driven through the membrane pores by the imposed pressure difference leaving the aqueous solution behind in the top portion of the device. Adapted from **Ref. 25** with permission from The Royal Society of Chemistry.

dependent on the hydrophobicity of the membrane along with the density and size of the pores. Having smaller pore diameter (~0.5 μm) is crucial in managing the efficiency of phase transfer. The small dimension of the pores allows high capillary pressures to force the transfer of the organic phase exclusively from the original mixture. In a successful application, the liquid-liquid extractor unit was used for continuous preparation of aliskiren, a common pharmaceutical. The combined production and purification of aliskerin was achieved for 100 h at a rate of 40 g/h[26]. The only disadvantage with this specific process was that, over time, the integrity of the Teflon membrane deteriorated either by contamination or structural damage.

Recently, Campos et al. described a membrane-less electroextraction unit, which separates compounds based on differences in their electrophoretic mobility and solvent affinity. Here, two physical properties are exploited to achieve efficient extraction using an aqueous two-phase system (ATPS)[27]. Being a relatively new technique, ATPS is not as commonly used as aqueous-organic liquid-liquid extraction. ATPS ,however, can be applied to a versatile library of analytes with potentially higher extraction efficiency[28].

Regardless of the manner of liquid extraction, contamination can be difficult to avoid due to incomplete extraction during the purification process. Extraction becomes even more challenging when purifying multiple targets, particularly if they exhibit different solubilities. Such a scenario could require significant optimization and multiple tandem extraction units that process different solvents, depending on the target solute. In one case, optimizing the extraction of a single solute required six identical liquid-liquid extraction units in series[29]. There is a continuing effort towards optimizing stable mechanisms of liquid-liquid extraction for future industrial applications, and a recent review highlights the current research[30].

1.4.3 Magnetophoresis

Particles that are naturally magnetic or functionalized with a magnetic tag can be separated from a sample in the presence of a magnetic field. Larger magnetic particles (micrometer and greater) are more susceptible to the force applied by a magnetic field. Since very few particles exhibit magnetic properties, efficient separation can be achieved with minimal contamination. Free-flow magnetophoresis separates particle analytes from a stream of sample, which is driven continuously through a magnetic field and typically orientated orthogonally to the flow. Magnetophoresis, in free-flow form, has been applied to the separation of cancer cells from normal cells[31,32], DNA purification[33], water purification[34,35], and nanoparticle purification[36].

Aside from being an efficient and precise means of separation, steady-state performance is easily achieved in magnetophoresis, which is an attractive advantage for continuous-flow purification. One caveat, however, is that magnetophoresis in small channels is prone to clogging. The removal or prevention of a clog would require the magnetic field to be weakened or turned off. If this occurred in an integrated CFC design, magnetophoresis would force the entire process to a halt. Furthermore, since very few analytes can be resolved naturally by magnetophoresis, all other analytes would have to be labelled with different magnetic tags in order to achieve separation. In CFC, such labeling would follow a flow reactor and must be extremely selective, making a tandem continuous-flow synthesis and purification setup highly impractical.

1.4.4 Free-Flow Electrophoresis

Free-flow electrophoresis (FFE) continuously separates target molecules from a sample that is exposed to an electric field **(Figure 1.4)**. The electric field is directed orthogonally to a pressure-driven hydrodynamic electrolyte flow, which carries the sample. The lateral separation of components is determined by: differences in their electrophoretic mobilities, the strength of the electric field, and the

speed of the hydrodynamic flow. FFE was originally used to continuously purify large volumes of complex biological samples. Furthermore, in this application the components of a FFE device were reusable for different samples. These advantages demonstrated that FFE was a viable high-throughput preparative platform, at least for the mentioned application.

FFE devices can be classified into four categories based on their scale: macroscale[37], midscale [38], milliscale (mFFE)[39], and microscale (μFFE)[40]. The scale categories are mainly defined by the volumes of the separation channels but are also characterized by acceptable ranges of flow rates and electric field strengths **(Table 1.1)**. The lower range of flow rates employed by macro, mid, and mFFE devices are comparable because of the similarity of their separation channel heights. In general, sample flow rate conditions used in FFE devices depend on the type of sample that is being separated (i.e. large analytes, like cells, require higher flow rates), and background electrolyte flow rate. It is worth mentioning that the maximum electric field strength is defined not by the gross size of the device or the separation channel, but mainly by the dimension of the separation channel height and the resultant ability to efficiently

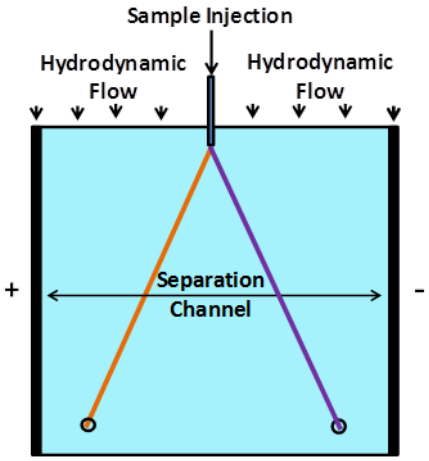

Figure 1.4: A simple schematic illustration of FFE. A continuous hydrodynamic electrolyte flow carries a sample through a wide separation channel. The sample is separated by an electric field into its individual components. The migration of each component is dependent on its respective electrophoretic mobility.

Table 1.1: Defining parameters of various FFE scales used as a preparative technique. Unless referenced otherwise, the parameters were extracted from the literature source listed under "Device".

Device	Maximum volume of separation channel (mL)	Range of sample flow rate (µL/min)	Maximum electric field strength (V/cm)	Aspect (width to height) ratio	Surface area to volume ratio (mm^{-1})
Macro-scale FFE[37]	35.7	6 – 97	250	143	1.4
Midscale FFE[38]	1.89	5.4 – 18.6	140	85	2.9
mFFE[39]	1.32	4 – 600	100[41]	300	5
µFFE[40]	0.025	0.08 – 4	708[42]	400	20

dissipate heat through the top and bottom plates of the device. The midscale and macroscale FFE devices employed higher electric field strengths than mFFE due to an efficient cooling liquid strategy which mitigates Joule heating. I chose the optimal separation conditions from each scale where a FFE device was used as a preparative technique and, thus, potentially capable of high-throughput CFP.

Up until now, I have described only one possible mode of FFE separation. **Figure 1.4** illustrates the most elementary example of FFE operation, which is called free-flow zone electrophoresis (FFZE). FFZE, however, may not provide optimal separation conditions for all samples. Certain samples can be separated more efficiently by other FFE analogues. These analogues include: free-flow iso-electric focusing (FFIEF); free-flow isotachophoresis (FFITP); free-flow field-step electrophoresis (FFFSE); and free-flow interval zone electrophoresis (FFIZE) (**Figure 1.5**). The parameters highlighted in **Table 1.1** would not differ greatly between analogues, as the listed parameters define the physical dimensions of each scale and their respective maximum electric field strengths and flow rates. Each analogue has its advantages and could likely be integrated into CFC technology. Here, I will briefly introduce them.

1.4.4.1 Free-Flow Iso-Electric Focusing (FFIEF)

Establishing a pH gradient is necessary for FFIEF, as the gradient enhances separation by focusing sample components into narrow pH regions. Ampholytes, which are added to the buffer, create

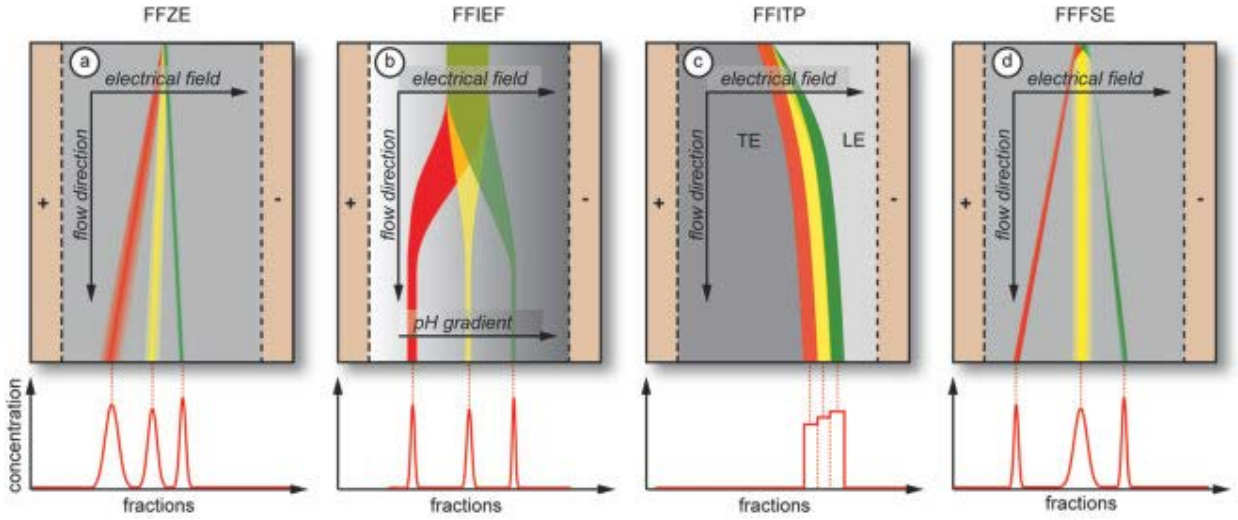

Figure 1.5 Modes of FFE: (a) FFZE, (b) FFIEF, (c) FFITP, and (d) FFFSE. Reproduced from **Ref 43** with permission from Wiley.

the pH gradient once a voltage is applied. Ampholytes, by definition, are zwitterions and will migrate in an electric field until reaching their isoelectric point; where the pI of an ampholyte is equal to the pH. The ampholytes can be selected to cover a broad or narrow pH range. The pH gradient is a time dependent process as the ampholytes rearrange themselves to create the gradient.[43]

When FFZE is operated at a uniform pH, separation of ampholytes is difficult as it can lead to significant band broadening. FFIEF, however, counters band broadening through focusing and is, therefore, perfectly suited for the resolution of ampholytic species. FFIEF is used extensively for the purification of proteins or peptides. With a stable and well defined pH gradient, FFIEF can easily purify a complex mixture of multiple proteins. The resolving power of FFIEF is comparable if not better than HPLC for this reason. One precaution is the potential denaturation of proteins as they migrates across a pH gradient; especially if the purpose is preparative purification where a functional protein is required.

1.4.4.2 Free-Flow Isotachophoresis (FFITP)

FFITP is less common than FFIEF; however, the focusing principle is similar. In order to properly focus, two buffers, which possess faster and slower mobilities than the target analyte, are used. The faster

and slower buffers are called the leading and terminating electrolytes, respectively, and sheathe the analyte on either side. The result is that the analyte, with the intermediate mobility, will focus at the boundary of the two buffers, thus, separating it from the sample. Typically, FFITP would be introduced in order to pre-concentrate one analyte with high recovery. Pre-concentration can be achieved rapidly using FFITP, and would be an attractive means of purification when large volumes of sample are introduced by high flow rates.

1.4.4.3 Free-Flow Field-Step Electrophoresis (FFFSE)

An alternative to FFITP is FFFSE, where focusing is achieved at the edges of the separation channel. Buffers, with higher conductivity than the analytes, are introduced near the edges of the separation channel, thus, allowing the same focusing event. This allows FFFSE an additional advantage of resolving multiple species as well as focusing them. An important advantage associated with the use of FFITP and FFFSE is high-throughput capabilities of large sample volumes and the ability to introduce sample at high flow rates. Typically, high sample flow rates are responsible for causing sample dispersion.

1.4.4.4 Free-Flow Interval Zone Electrophoresis (FFIZE)

The final important variation of FFE is FFIZE and was introduced by Bauer and Weber in 1998[44] (**Figure 1.6**). In this platform, a sample is injected into a FFE device and passed through the separation channel in the absence of an electric field. Once the sample spans the entire length of the separation channel, the hydrodynamic flow is turned off and a voltage applied. Here, the components of the sample are separated laterally from each other along the width of the separation channel. After separation has been achieved, the flow is re-established and the components are collected from outlets at the end of the separation channel.[45] The true benefits of FFIZE were revealed in a quantitative study in 2012. It was demonstrated that FFE separation power could be increased by reducing band broadening caused by the

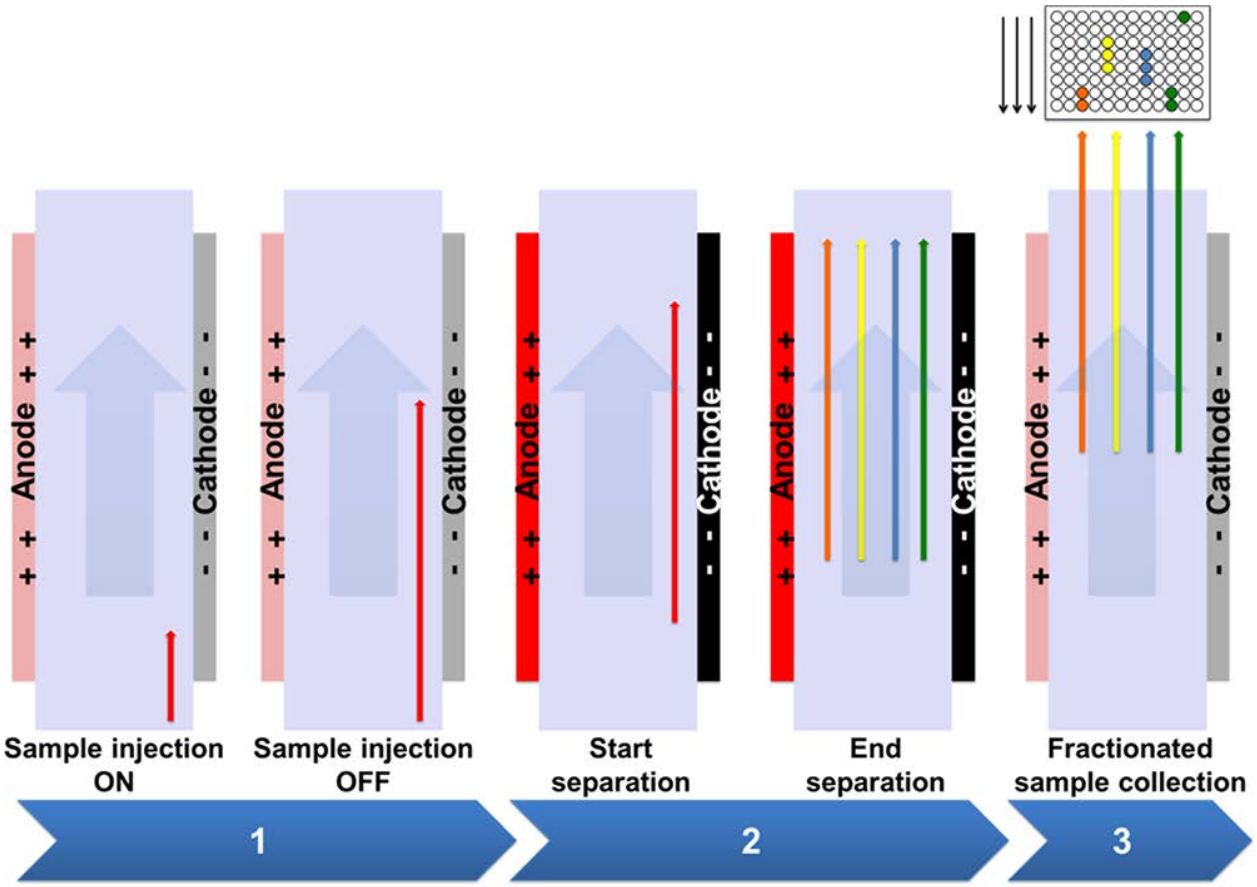

Figure 1.6: Free flow interval zone electrophoresis (FFIZE), and schematics of the FFIZE separation process. (Step 1) Sample is injected into the continuous laminar flow and allowed to continue into the chamber. (Step 2) The electrical field is applied in an optional time interval depending on the electric mobility of the compound of interest. (Step 3) After separation of the sample, fractions are collected. Adapted with permission from Justesen, B. H.; Laursen, T.; Weber, G.; Fuglsang, A. T.; Moeller, B. L.; Gunther Pomorski, T. Anal. Chem. 2013, 85, 3497. Copyright 2013 American Chemical Society.

simultaneous effects of electrophoresis and hydrodynamic flow[46]. While interval FFE is an effective way to increase separation power, the platform becomes a combination of discontinuous flow and discontinuous separation. Thus, it is difficult to consider FFIZE as a complement to CFS.

1.5 Limitations Associated with CFC-FFE Integration and Achieving Steady-State Purification

While being the driving force of separation in electrophoresis, an electric field creates a number of problems that prevent the use of small-scale (milli-, mid-, and micro-scale) FFE for steady-state CFP. The electric field affects steady-state purification by three associated mechanisms: Joule heating, bubble

generation, and the H^+/OH^- transport that forms pH gradients. To date, the regeneration of a steady-state typically requires frequent shutting down of a device, which is not a viable option for integrated CFC.

Macroscale FFE could be a good candidate for CFC integration. Aside from compatible flow rates, macroscale FFE is a rugged and reliable technique, as is evident in commercial devices (such as Octopus)[47], which have existed since before the 21st century. Such devices have high-throughput capabilities, high separation power, and well established steady-state purification strategies. A major caveat with respect to macroscale FFE integration to CFC, however, is that macroscale FFE dimensions are large (separation channel volume in **Table 1.1**). As a result, these devices consume large volumes of sample and reagents, and the residence time of samples can also be large. The essence of CFC, especially CFS, is to minimize waste and maximize efficiency, which can be achieved through small-scale processing. The miniaturization of FFE has certain attractive attributes, such as small volumes, efficient heat and mass transfer, and facile on-line detection schemes, thus, making midscale and mFFE more practical for CFC integration. Midscale and mFFE, however, are not nearly as reliable purification techniques as their larger counterpart. Scaling FFE from the macroscale down to smaller dimensions incorporates a significant limitation: the need to address, *de novo*, all issues of instability. While macroscale FFE performance has solved the problems that prevent steady-state purification, its strategies are not easily transferrable.

The goal of this dissertation was to provide solutions that can allow steady-state continuous-flow purification using FFE at scales other than macroscale FFE. Here, I propose the development of a mFFE device that can be easily integrated with CFS micro-reactors. Preliminary mFFE fabrication should be rapid and reproducible in order to expedite device optimization. I had access to a robotic milling machine that has the capacity to manufacture individual mFFE devices within 24 hours. Steady-state issues can then be addressed with a working mFFE prototype. To achieve steady-state optimization I developed innovative geometric modifications, which were validated with multiphysics simulations using COMSOL.

I then used the optimized geometry to minimize the adverse effects associated with bubbles and pH gradients over a broad range of separation conditions, and over long periods of time.

CHAPTER 2: RAPID PROTOTYPING OF mFFE DEVICES

The presented material was published previously. Adapted with permission from:
Agostino, F.J.; Evenhuis, C.J.; Krylov, S.N. Milli-free flow electrophoresis (mFFE): I. Fast prototyping of mFFE devices. *Journal of Separation Science*, **2011**, 34, 556-564.

Contributions to the article: fabricated all mFFE devices, performed all experiments, first author of the manuscript, and prepared figures.

2.1 Introduction

Continuous flow microreactors are an attractive means of synthesis. Compared to batch synthesis, they offer: an appreciable increase in product yields through atom economy[48]; reduced costs associated with starting materials; safer operating conditions and better control[49], and the capacity to generate high throughput production by numbering up[50], in which parallel processing units can be combined to achieve larger scale performance. Progress in this area has been slowed by the lack of a compatible continuous purification technique. In principle, FFE would be suitable as a separation technique, but has not yet been widely accepted[51].

To date, there is only one example of where µFFE has been successfully integrated in a CFC design. An in-line µFFE device was used to purify three amino acids that were derivatised continuously with a chromophore in a micro-reactor[52]. In general, however, µFFE flow rates are too small for high-throughput preparative technology and do not reflect flow rates that are typically used in continuous-flow micro-reactors. Typical flow rates used in continuous flow microreactors are within the range of 5–2000 µL/min[49,53-56]. These flow rates have been optimized to acquire the high yields that microreactors produce. The flow rates used in larger scale FFE are compatible with the flow rates in most continuous-flow micro-reactors, making these purification scales better suited for CFC design. The work presented in this dissertation focused on the revival of midscale FFE. Such a scale offers the high-throughput advantages of macro-scale FFE but without the need to consume large volumes of buffer, or potentially long separation times.

In 1975, Hannig et al. produced a midscale FFE device with dimensions intermediate to macro-FFE and mFFE[37]. The mid-scale alternative was used successfully to separate proteins as well as to evaluate a number of electrophoretic parameters[38]. I proposed the prototyping of a midscale FFE device that would be compatible with microreactors; called ‘‘milli’’-FFE (mFFE). mFFE has the potential for high-throughput continuous purification in line with continuous flow microsynthesis, while conserving the essence of Green Chemistry.

To explore CFS-mFFE integration, multiple mFFE prototypes need to be fabricated in a timely and cost-effective fashion. Modern methods of fabrication include photolithography, hot embossing, and laser ablation; however, they are neither suitable for rapid prototyping, nor are they suitable for fabricating scales larger than μFFE. The first two methods are costly and time consuming to implement and laser ablation is limited by the complexity that can be integrated into potential designs[57,58]. Using photolithography to fabricate larger scale devices would only incur higher costs, and would be technically impractical for creating millimetre dimensions. Milling machines, however, have the capacity to reproducibly remove material, and to prototype complex geometries rapidly and at low cost. They have been used previously to manufacture microfluidic devices[59-61]. For mFFE, milling is an ideal method for prototyping devices at this scale. Here, for the first time is the demonstration of the prototyping of an mFFE device using a milling machine. A solution bonding technique is used to irreversibly seal two poly(methyl methacrylate) (PMMA) substrates together in less than 10 min. Combining the fast prototyping capabilities of a milling machine with rapid bonding can produce a fully functional device in less than 24 h. Much work was involved to optimize this procedure and to successfully produce a functional mFFE device. This chapter concisely informs readers of the optimal parameters needed to reproduce this work. More importantly, with this knowledge prototyping is accelerated and the potential for in line continuous purification of CFS products is significantly enhanced.

2.2 mFFE Assembly

2.2.1 Optimization of Milling

Tools of all diameters and shapes can be installed in a milling machine to perform the numerous operations that make milling such a versatile and useful method of fabrication. Each operation is unique in that it can reproducibly remove stock material, profile the dimensions into the stock, and flatten the surface to make it smooth. Teamed with this high precision, the milling machine can make incisions that are less than 500 μm in width. Technically, the milling machine also permits depths of as little as 1 μm, but at a risk of its precision. Thus, it is possible to achieve micrometer dimensions in at least one direction.

Preparing a mFFE device can be achieved in less than 24 h. **Figure 2.1** demonstrates the efficiency of milling machine device fabrication. Solid Edge software is user friendly and contains tutorials for new users to become familiar with designing shaped devices. Modeling mFFE designs was a simple task and could be completed within an hour. Adjusting existing designs was intuitive and required only minutes. Calibration and milling preparation were critical to the entire procedure. Placing the PMMA stock in the milling machine was important in order to accurately match the frame of reference designed by Edge Cam. Marking the stock was helpful in attaining accurate orientation.

Fabricating the top and bottom substrates required 11 h to complete. The total time including modeling, calibration, fabrication, bonding, and assembly was 14 h. This time is quoted for an experienced milling machine user; however, for a novice user, the time required should still be under 24 h. Time can be managed more efficiently with instrumental accessories. One such accessory is the automatic cutting tool changer, thus, reducing installation time and also monitoring time.

Great amounts of caution were exercised when roughing with the ⅜” cutting tool. The reason for this additional care was to eliminate the adverse effects of excessive force and vibrations associated with this tool. In certain cases, the ⅜” cutting tool is capable of pushing so strongly in the vertical direction that

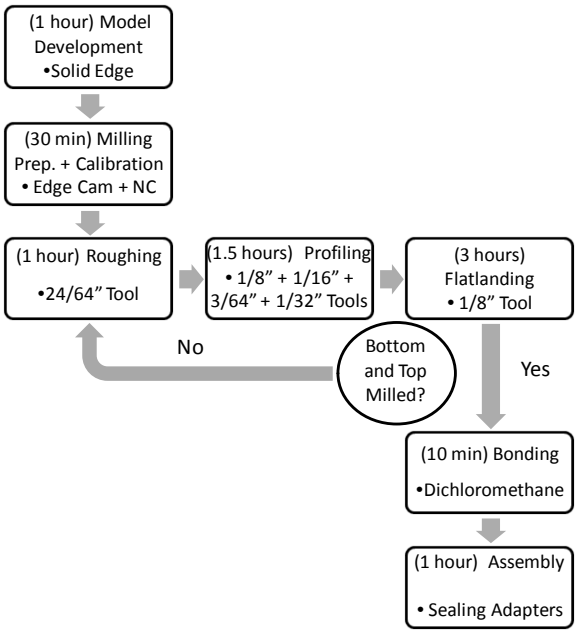

Figure 2.1: mFFE Fabrication with a milling machine

it could shift the stock downward; this compromises the precision associated with the milling machine. To correct for this issue, I use a solid piece of aluminum as support below the substrate. Also, reducing the cut increment limits the amount of material through which a tool would drill.

If a procedural error is experienced during milling, it takes little time to correct the problem. Milling machines are convenient in that they can re-start an operation at exactly the same place as where they left off. All calibrations are saved and the only setback is to replace the PMMA substrate into the milling machine. Fabrication with the milling machine allowed consistent monitoring, which was a significant benefit for efficient prototyping. Whereas the success of fabricating with other techniques cannot be determined until after fabrication or until after the device has been used.

2.2.2 Optical Transparency and Clarity of PMMA

Optimizing the ‘‘milli’’-chip itself involved reproducible fabrication of mFFE devices that were flat and optically transparent. This was achieved by optimizing the flatlanding operation. The variation of

transparency and optical clarity with flatlanding conditions is illustrated in **Figures 2.2 and 2.3**, respectively. In both figures, panels **A**–**D** depict the same milling conditions. In **Figure 2.2**, the optical transparency of **A**–**D** is compared. Light scattering is attributed to the substantial increase in absorbance

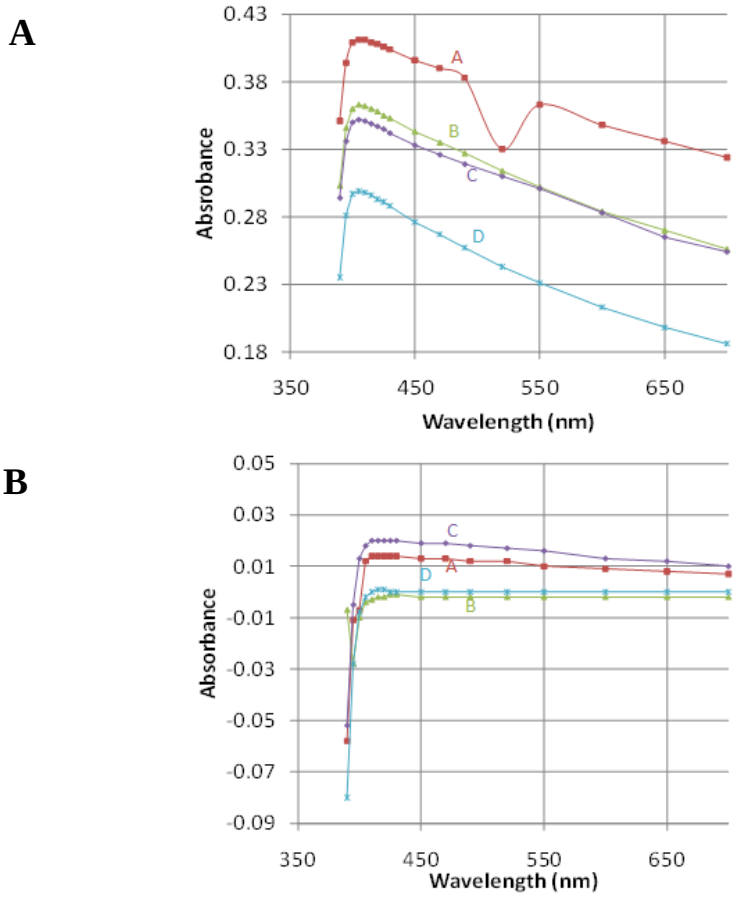

Figure 2.2: The absorbance of milled PMMA relative to a nonmilled piece of PMMA. The differences in measured absorbance reflect the scattering of light. The tool diameters (inches), feed rates (mm/min), and rotational frequencies (revolutions per minute) were used, respectively: (**A**) ; Ø = $^{1}/_{32}$, FR = 800, rpm = 10^4; (**B**) ; Ø = $^{1}/_{32}$, FR = 150, rpm = 6×10^3; (**C**) ; Ø = ⅛, FR = 800, rpm = 10^4; and (**D**) ; Ø = ⅛, FR = 200, rpm = 3×10^3. The top graph refers to PMMA pieces that were not coated with mineral oil, and the bottom graph refers to PMMA pieces coated with mineral oil.

for the pieces that were poorly flatlanded. Using faster feed rates (FR) and rpm, in **A** and **C**, resulted in rough and optica lly obstructed surfaces. At FR = 800 mm/min, the tool does not have sufficient time to properly smooth the surface, and at rpm = 10^4 the tool can potentially melt the surface creating translucence. Melting of PMMA was a significant issue. It not only compromised the optical quality of

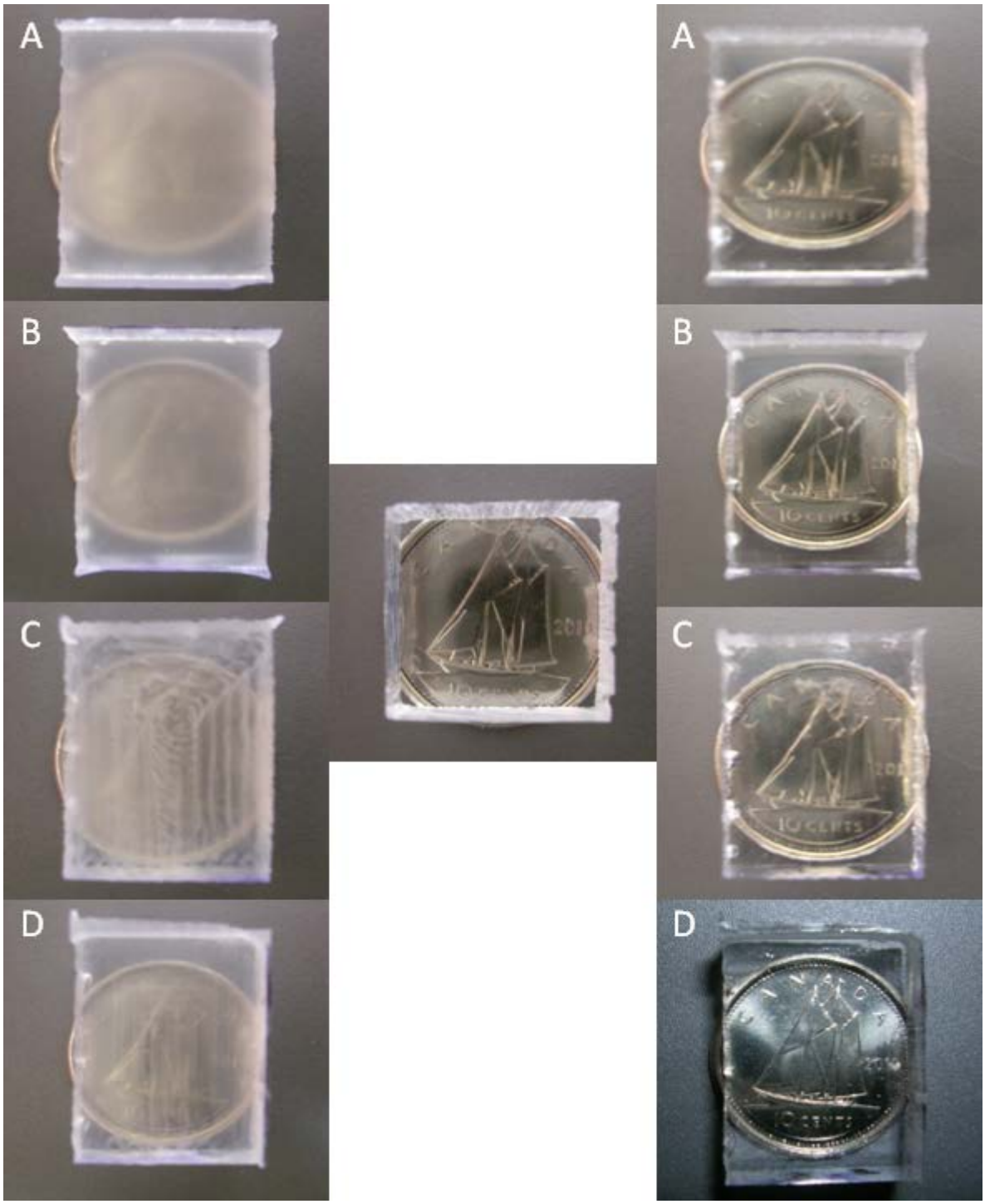

Figure 2.3: Optical clarity of PMMA. The differences in flatlanding parameters alter the PMMA clarity. At the center is a non-milled piece of PMMA, behind which is a Canadian dime. The panels on the left show the PMMA pieces before coating with mineral oil, and the panels on the right show PMMA pieces coated with mineral oil. The milling conditions compared here are identical to those used in **Fig. 2.2**.

the surface but melted plastic could accumulate on the surface of the cutting tool making them susceptible to breakage. This was circumvented by decreasing the rpm, and by subjecting the tool to a stream of pressurized air during milling. Using smaller tools, in **A** and **B**, produced the least favorable optical quality as it generated clouded surfaces, a result of melting. The optimal surface clarity, in **D**, was achieved using the ⅛" tool, FR = 200 mm/min and rpm = 3×10^3. Similar results were achieved in **Figure 2.3** when comparing the optical clarity of the pieces. Optical optimization was an important aspect of mFFE prototyping, especially using visual detection.

2.2.3 Solution Bonding

Sealing two PMMA substrates with dichloromethane proved to be an efficient method of bonding, and a rapid means of preparing microfluidic devices. One goal of this work was to develop an efficient means of prototyping devices, and solution bonding proved an exceptional complement to milling. It was solution bonding that allowed prototyping to be accomplished within a 24 h period. There is no significant optimization associated with this technique, as there can be for thermal bonding. Thermal bonding is tedious to optimize as it is necessary to find an ideal balance between three variables: pressure, temperature, and time[62,63]. Without the necessary thermal bonding optimization there is a risk of channel deformation or clogging. Adhesive bonding works in a similar fashion to solution bonding in that the curing time is comparable. However, one important limitation is that it introduces an increase in height of the separation channel due to the layer of adhesive. For the sake of reproducible microfluidic flows, any additional height is unfavorable and can have adverse effects.

In the solution bonding approach the top and bottom PMMA substrates are not identical but have individual features to facilitate bonding between the two faces, and to aid in the proper fitting of the two substrates. The first feature is a protrusion on one side of the face and the second is a complementary cutout wherein the protrusion would fit tightly. This relationship is called a ‘‘snap fit’’. Solution bonding

is ideal in that dichloromethane (CH_2Cl_2) is added after the device is connected by the “snap fits”. The channels developed specifically for solution bonding worked perfectly to seal the surfaces together and do not disturb the rest of the device. This is attributed to the orientation of the bonding channels; they are outside of the locations of the ‘‘snap fit’’ and separation channel. The ‘‘snap fit’’ assembly greatly assists in bonding two pieces together. They work by lining up the two matching pieces perfectly. The use of the bonding channels and ‘‘snap fits’’ simplify the bonding process and prototyping overall.

The only risk associated with solution bonding, using CH_2Cl_2, is its possible penetration around the ‘‘snap fits’’ causing clogging of the separation channel and/or the loss of optical transparency. This could be circumvented by reducing the volume of dichloromethane used for bonding.

2.3 Improving the Quality of Separation

2.3.1 Bubble Elimination

Of the previously reported methods to limit the effect of bubbles on the electric field strength, the most successful technique was to increase the flow rate within the electrode channels[64]. Once the bubbles were generated, the increased flow rate removed them rapidly preventing them from entering the separation channel and, more importantly, interfering with the electric field. **Figure 2.4** demonstrates by simply increasing the depth of the electrode channels from 1.0 mm, in which the electrode occupied a substantial fraction of the electrode channel, to 1.5 mm, the bubbles generated by electrolysis were effectively prevented from entering the separation channel. Adjusting the height of the electrode channels was facile using the milling machine. This obviated the need to add membranes to separate the electrodes from the separation channel[40,65], or the need to add redox additives to the buffer surrounding the electrodes[66].

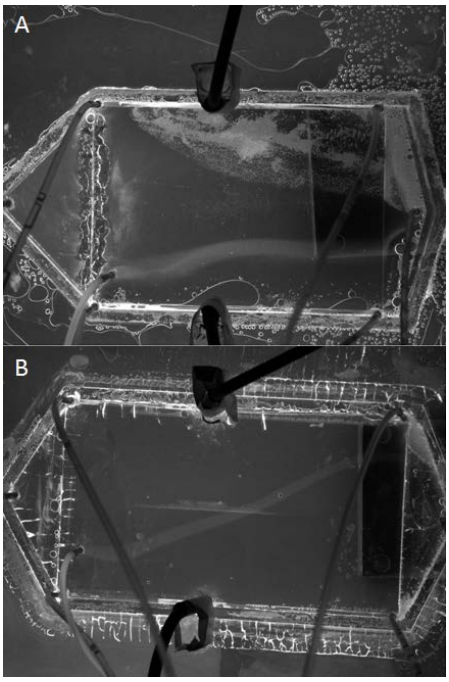

Figure 2.4: Bubble elimination by increasing channel depth. The applied voltage was 800 V (E = 133 V/cm) to deflect fluorescein. The electrode channel depths were (A) 1.00 mm and (B) 1.50 mm. Flow rate =0.66 mL/min

2.3.2 Achieving Laminar Flow

Despite the large size of this FFE device, the 200 μm separation channel depth allows laminar flow to exist. This is illustrated by calculating the Reynolds number for the flow within the separation channel. A Reynolds number less than 2000 indicates laminar flow.

$$Re = \frac{\rho v H}{\eta} \tag{2.1}$$

where Re is the Reynolds number, ρ is the fluid's density, v is the hydrodynamic velocity, η is the viscosity and H is the height of the separation channel. All values for the buffer are approximated to that of water at 20°C.

$$Re = \frac{(1000\ \mathrm{kg\,m^{-3}})(9.2\ \times 10^{-4}\mathrm{m\,s^{-1}})(2.0\ \times 10^{-4}\mathrm{m})}{(1.002\ \times 10^{-3}\ \mathrm{kg\,m^{-1}s^{-1}})} = 0.18 \tag{2.2}$$

The calculated value of 0.18 for *Re* is well within the laminar realm. The sample enters the separation channel at a point where laminar flow is already established. Diffusional band broadening is limited by the relatively short time spent by the sample in the separation channel.

2.3.3 Ideal Positioning and Diameter of the Sample Inlet

Originally, the sample inlet was positioned closer to the electrode channel, and the dimensions of the entrance and exit reservoirs were rectangular. This decreased the control of the sample stream trajectory. The fast flow rate in the electrode channel influenced the direction of the sample; as a result it traversed into the electrode channel in the absence of an electric field. This effect was observed earlier by Fonslow and Bowser, and maintaining linear sample streams was achieved by using triangular entrance and exit reservoirs[67]. Repositioning the sample inlet at the center of the separation channel adds versatility with respect to the possible types of separation. Having already achieved laminar flow, the cause of band broadening is associated with the dimension of the sample inlet. By reducing its diameter from 1.8 to 0.75 mm, the sample stream widths were reduced substantially, thereby improving resolution.

2.3.4 Flow Control with a Syringe Pump

The first resolution experiments were performed using gravity to push the sample into the separation channel. Using gravity, however, resulted in limited control of a consistent flow rate. The sample flow rate was halted upon the application of an electric field, regardless of the electric field strength. The generation of bubbles could be responsible for this effect, because the pressure created by their presence causes a backpressure in the sample capillary. This could be resolved by increasing the height of the sample stock; however, this required precise optimization of the sample height. Unfortunately, the removal of bubbles is not as fast as their generation, thus achieving a consistent sample flow rate was exasperating. The use of a syringe pump easily rectified this issue, as it precisely supplies a

consistent flow rate. The application of an electric field did not adversely affect the sample stream or flow rate. This allowed resolution to be optimized over a precise range of sample flow rates.

2.3.5 Separation of Fluorescein from Rhodamine B

A successful separation of fluorescein and rhodamine B was achieved soon after the optimizations of bubble elimination and laminar flow and trajectory (**Fig. 2.5**). The two dyes were spatially resolved after applying only 400 V (67 V/cm), with a resolution, R_s = 9.5. The two streams were narrow and demonstrated little band broadening. The quality of the separation was maintained for at least 15 min without any disruption. After this time, the voltage was halted and the hydrodynamic flow was increased sufficiently for 30 s to remove the bubbles from the electrode channels, and regenerate the same separation conditions as before. Closer to the exit reservoir, both streams were deflected toward the center. This was a result of having only one outlet. The flow velocity profiles were influenced by the positions of both the inlet and outlet. The optimal sample flow rate introduced into the devices was 10 µL/min. This flow rate gave the best resolution and was compatible with the output from continuous flow

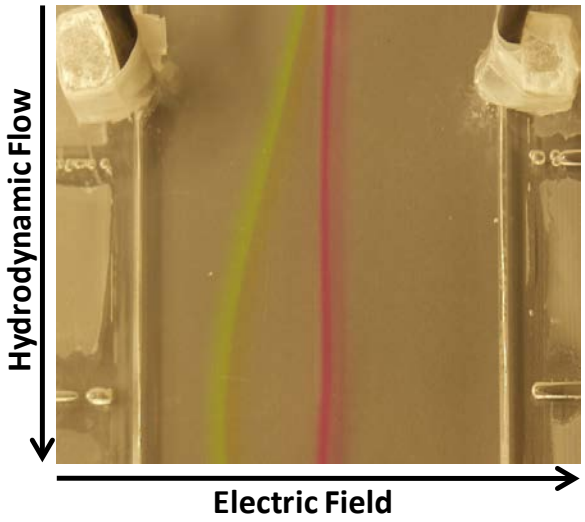

Figure 2.5: Successful resolution of rhodamine B and fluorescein. Separation voltage = 400 V (E = 67 V/cm), and the flow rate of buffer = 0.66 mL/min R_s = 9.5

microreactors. Furthermore, the scale at which mFFE exists has a number of potential benefits: efficient heat transfer supplied by high surface area to volume ratios; high-throughput capabilities within one device; cost-effective and rapid prototyping platform for microfluidic applications; and most importantly being compatible with microreactors for tandem CFS-CFP.

2.4 Concluding Remarks

This work reinforces the FFE area with a tool for fast prototyping of mFFE devices. Below I briefly outline the results. The fabrication and optimization of a fully functional ‘‘milli’’-free-flow electrophoresis device using a milling machine have been demonstrated. Fluorescein was resolved from rhodamine B at 400 V (67 V/cm), $R_S = 9.5$. A milling machine was used to manufacture the device in less than 24 h. Solution bonding with CH_2Cl_2 sealed two PMMA substrates in less than 10 min without any leaking or channel deformation. Stable, laminar flow of sample was achieved using a syringe pump. The sample flow rates administered in the ‘‘milli’’-chip can be compatible with most continuous flow microreactors. mFFE would serve as a complementary means of CFP. As a method of prototyping, milling offers an inexpensive and time-efficient alternative to modern microfabrication techniques based on photolithography, hot embossing or laser ablation, whenever larger devices are involved. By following the protocols described in this chapter, practitioners will be able to design manufacture and test devices in a much shorter time frame than previously experienced.

2.5 Materials and Methods

2.5.1 Solid Edge

All FFE models were designed using Solid Edge (Siemens PLM, Plano, TX) software. Starting with a 3-D base, features were modeled as 2-D sketches on the surface of the base. The 2-D sketches included a separation channel (60 × 110 mm), two electrode channels (1.5 × 110 mm), triangular exit and entrance reservoirs (60 × 10 mm), circular buffer inlets and outlets (1.8 mm diameter), circular electrode holes (1.8 mm diameter), and circular bubble outlets (3.6 mm diameter). **Figure 2.6** illustrates the setup for this FFE device. These sketches were modified by height or depth by applying a protrusion or cutout function, respectively. The separation channel was 200 µm deep, the electrode channels were 1.15 mm deep, the reservoirs were 0.6 mm deep, and all of the holes were 5 mm deep. These modifications gave the FFE device its defining features. The cutout of the ‘‘snap fit’’ bordered the functional area of the FFE device and was 4 mm wide and 2.5 mm deep. Conversely the protrusion of the ‘‘snap fit’’ was 3.75 mm wide and 2.5 mm high.

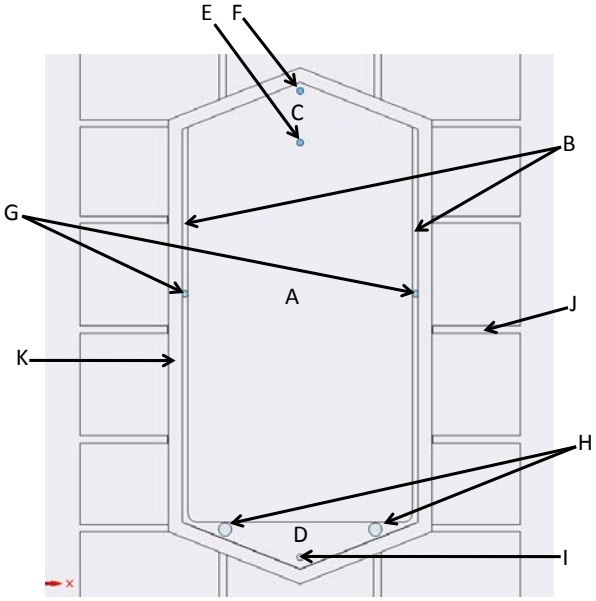

Figure 2.6: Top Substrate of FFE device. (**A**) Separation Channel, (**B**) Electrode Channel, (**C**) Entrance Reservoir, (**D**) Exit Reservoir, (**E**) Sample Inlet, (**F**) Buffer Inlet, (**G**) Electrode Holes, (**H**) Bubble Outlet, (**I**) Buffer Outlet, (**J**) Solution Bonding Channels, and (**K**) “Snap Fit”.

The third feature was a combination of narrow channels beginning at the edge of the base and touching the edge of the snap fit. These features existed on both faces, and were aligned with each other so that the combined channels were 2mm wide and 2mm deep. This depth was chosen so that a long syringe would be able to inject a bonding agent at the snap fit. The fourth feature was two extensions of the device from the base, or wire frames. Their purpose was to act as a support during milling.

2.5.2 Edge Cam and Numerical Control Coding

After Solid Edge designing, the model was exported to Edge Cam (Planit CAD/CAM Software, Tuscaloosa, AL), which is a preparatory software program for milling. In Edge Cam, the piece to be milled was modeled inside a simulated stock material. This stock was created by defining the distance (in mm) between the edges of the stock material and the FFE device. Once the orientation was organized, all defining features were recognized on the model through a ‘‘feature finder’’ function. Boundaries were then established to limit milling to specific regions.

The next phase was to prepare milling operations for the features defined within the boundaries. The three operations that were prepared were: roughing, profiling, and flatlanding. Important parameters were set up to control the milling accuracy: the FR; plunge rates; cut increments; and rotational speeds (rpm). The FR is the speed at which the tool traverses along the stock material, the plunge rate is the speed at which the tool traverses in a vertical direction, and the cut increment is the depth at which the tool will cut with each successive pass of the drill.

An MDX-540 milling machine (Roland DGA, Irvine, CA) was used to fabricate each device. Roughing removed the bulk material from the stock. The bulk is only removed by verifying the presence of excess stock. By default, Edge Cam assumed that excess stock material has already been removed. If this was not clarified before initiating the operation, the cutting tool would not have recognized its

absence and would begin to mill deeper into the stock, potentially damaging the model or the cutting tool itself.

Profiling was the most important operation, as it was responsible for defining the features of the device. Flatlanding was typically a final operation, which created smooth surfaces and removed any remaining stock to achieve the desired depth. Once each milling operation was prepared, numerical control (NC) codes were generated. Numerical control codes are deciphered by the milling machine to execute the operations. PMMA (Johnston Industrial Plastics, Toronto, Canada) was the substrate used to fabricate each FFE device. **Table 2.1** gives a summary of the optimal milling parameters. These values are the optimal values that have been established over the length of this project, and may not reflect the first values that were used in fabricating the initial mFFE prototype. Each tool (McMaster Carr, Chicago, USA) had its respective role in fabricating the FFE device. Before each operation, the cutting tool was installed into the milling machine and calibrated with respect to its depth. All of the cutting tools were reused. By applying due vigilance, multiple devices were fabricated without breakage. The cost of purchasing the five cutting tools was $200 (CAN). The cost of the PMMA for each device was approximately $10 (CAN). That was the total price of fabrication.

2.5.3 Order (of tooling) in Milling

Each tool had a threshold at which it would break. Using the tools in proper order reduced damage or breakage of the stock material and the tools themselves. Each cutting tool, largest to smallest, performed its milling functions before moving to the next tool. Roughing was always the first operation to be executed. The z-offset was set to a tolerance of 0.25 mm, allowing the ⅜” cutting tool to remove material to 0.25 mm from the actual surface of the device. The ⅛” and smaller cutting tools were used for the subsequent profiling operations. In this case no tolerance was programmed so to allow each cutting tool to reach the desired depth.

Flatlanding was performed immediately after profiling with the ⅛" cutting tool, effectively removing any remaining stock material left behind by the ⅜" cutting tool, and smoothing the surface. This limited any unnecessary strain on the smaller cutting tools by reducing the depths that these tools need to reach, due to the default assumption that there was no excess material present. If flatlanding was not performed, the smaller tools would mill through this excess material, potentially damaging or breaking the cutting tool.

2.5.4 Optical Transparency and Clarity

A UV-Vis spectrophotometer (Beckman Coulter, Oakville, Canada) was used to measure the absorbance (from 400 – 700 nm) of a variety of PMMA pieces flatlanded by the milling machine. The results were compared with a PMMA piece that was not milled.

The clarity of the same PMMA pieces was evaluated visually by observing a coin placed behind

Table 2.1: Optimal Milling Parameters

	Operation		
	Roughing	Profiling	Flatlanding
Cutting tool diameter			
3/8"	FR: 1750 mm/min PR: 50 mm/min rpm: 1500	N/A	N/A
1/8"	N/A	FR: 800 mm/min PR: 50 mm/min RPM: 2000	FR: 500 mm/min PR: 50 mm/min RPM: 6000
1/16"	N/A	FR: 600 mm/min PR: 50 mm/min RPM: 3000	N/A
3/64"	N/A	FR: 500 mm/min PR: 50 mm/min RPM: 4000	N/A
1/32"	N/A	FR: 450 mm/min PR: 50 mm/min RPM: 4500	N/A

each piece. Again, the results were compared with a PMMA piece that was not milled. Both the transparency and clarity experiments were repeated after coating the pieces with mineral oil (Sigma-Aldrich, Oakville, Canada). This was to better represent the optical environment within the mFFE device.

2.5.5 Solution Bonding

All reagents were purchased from Sigma-Aldrich unless otherwise mentioned. CH_2Cl_2 was used to bond two pieces of PMMA together. CH_2Cl_2 was introduced slowly with a syringe into the specially designed channels and allowed to move along the snap fit. Each subsequent channel was filled with CH_2Cl_2 carefully and allowed to perfuse to the next channel until each channel was filled. The setup was clamped together and allowed to bond for 10 min.

2.5.6 Resolving Fluorescein and Rhodamine B

Two solutions were prepared for resolving fluorescein from rhodamine B. The buffer solution consisted of 25 mM 4-(2-hydroxyethyl)-1-piperazineethanesulfonic acid (HEPES) (99.5%) at pH 7.0. 0.01% Triton X-100 was added as a detergent. The buffer solution was then filtered with a Millipore Express Plus 0.22 mm filter (Milian, Gahanna, USA). The sample solution consisted of fluorescein and rhodamine B both diluted to 500 µM in the 25 mM HEPES solution.

Polyethylene pipette tips (200 µL) were used as fluidic adapters and polyethylene tubing was used to transfer the solutions from their stock to the FFE device. Loctite® 409 (Henkel, Mississauga, Canada) was used to seal the adapters to the device and allowed to cure for 1 h. Platinum electrodes were installed into the electrode channels and connected with insulated copper wires to a power source. The power source used was a high-voltage Electrophoresis Power Supply EPS 3501 XL (Amersham Pharmacia Biotech, New Jersey, USA). Any openings, holes, or extra spaces were filled with Loctite® to prevent leaks.

The hydrodynamic flow of buffer was driven by gravity. The HEPES solution was mounted at a position high enough to force a flow rate of 5 – 6 mL/min through the chip. The velocity of the sample was measured by observing the position of the sample stream through the separation channel over time. The flow rate of buffer through the separation channel was adjusted to 0.66 ± 0.02 mL/min. This translated to a buffer flow rate of 4.85 ± 0.14 mL/min in the electrode channels. The velocity of the sample stream was driven by a syringe pump (Harvard Apparatus Pump II, Saint-Laurent, Canada) and introduced at a rate of 10 μL/min.

Optical detection was achieved by using a CCD camera (Alphamager, San Francisco, USA). Fluorescence was induced by UV excitation (488 nm) (Alpha Innotech, Santa Clara, USA) and detected through a detector specific to fluorescein. At high concentrations of fluorescein and rhodamine B, a digital camera (Olympus E-10) mounted on a tripod was used to record images.

CHAPTER 3: STEADY-STATE CONTINUOUS-FLOW PURIFICATION BY ELECTROPHORESIS

The presented material was published previously. Adapted with permission from:
Agostino, F.J.; Cherney, L.T.; Galievsky, V.; and Krylov, S.N. Steady-State Continuous-Flow Purification by Electrophoresis, *Angewandte Chemie International Edition*, **2013**, 52, 7256-7260.

Contributions to the article: fabricated all mFFE devices, performed all experiments, first author of the manuscript, and helped prepared figures.

3.1 Introduction

FFE facilitates continuous separation of molecules in a wide separation channel with a uniform hydrodynamic flow of an electrolyte solution and an electrical field non-parallel (typically orthogonal) to this flow. The sample is introduced into the separation channel through a narrow opening as schematically shown in **Figure 3.1**. Advantageously, FFE devices can be made on scales to suit small flow rates used in continuous-flow microsynthesis. Unfortunately, small-scale FFE cannot be used for steady-state purification[68]. Electrolysis of water leads to the formation of O_2 and H_2 bubbles on the surface of the electrodes. Bubble accumulation on the electrodes and subsequently in other parts of the device leads to progressing electric-field distortion and diminishing quality of purification within the first several minutes of operation[69,70]. The regeneration of an FFE device requires complete bubble flush-out: a cumbersome and time consuming process. The goal of this work was to find a solution for the problem of FFE instability caused by bubble accumulation, thereby permitting reliable steady-state operation without the distortion of electric field or separation quality. Solving the bubble-accumulation problem is pivotal to FFE integration with other micro-systems[71].

The previous approaches to the problem of bubble accumulation in FFE devices could be split into three major categories: 1) a mechanical barrier preventing the entry of bubbles into the separation channel[65], 2) separate electrode channels with fast flow for bubble removal[64], and 3) chemical agents that

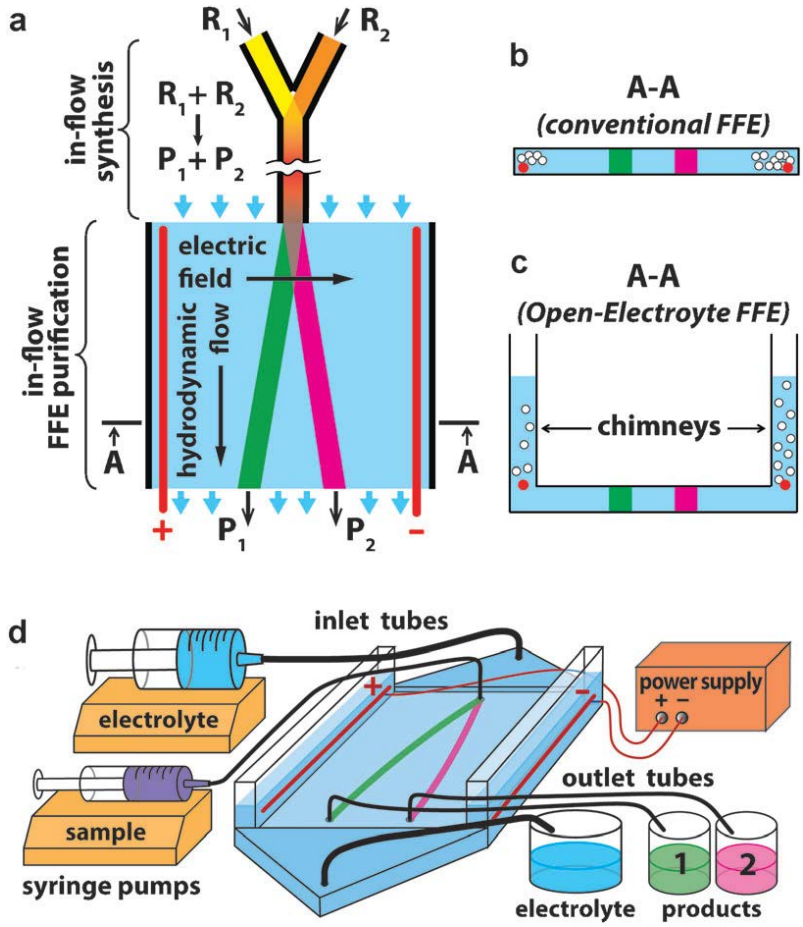

Figure 3.1: a) Schematic top view of an integrated system for continuous-flow microsynthesis and subsequent continuous-flow purification. The reactants, R1 and R2, generate products, P1 and P2, which are separated by FFE. A conceptual comparison of cross-sections (section A–A in panel (a)) in devices for conventional FFE (b) and our OEFFE (c). In OEFFE, bubbles (o) generated at the electrodes (red dot) are vented out of the device into the atmosphere through the chimneys. d) General overview of an OEFFE device.

inhibit gas generation and bubble growth[66]. While being useful, these measures only delay the accumulation of the deteriorating amount of bubbles. Bubbles still accumulate and prevent steady-state continuous separation. Because of bubble accumulation, electrical-current and sample-flow stability in μFFE typically lasts for less than 0.5 h. The mFFE device introduced in the previous chapter was operation for a maximum of 15 minutes. The longest operational time demonstrated for small-scale (micro or milli) FFE is 2 h[72].

This work was inspired by an insight that a solution to the bubble-accumulation problem could be achieved by breaking the principle of a closed FFE device. The logic was simple. Bubble removal into the

atmosphere could be easy and natural if the electrolyte above the electrodes was open to the atmosphere. Further, engineering the "open-concept" FFE device requires vertical chimneys to hold a column of electrolyte that hydrostatically balances the pressure inside the device. Since the Archimedes force pushes the gas upwards, bubble entry into the separation channel can be completely prevented by placing the electrodes in the chimneys above the level of the separation channel. This approach was termed open-electrolyte FFE (OEFFE). **Figure 3.1** schematically illustrates the differences between the classical planar FFE device (**Figure 3.1b**) and an OEFFE device with chimneys (**Figure 3.1c**). Ideally, the setup should be designed to include a way to collect sample fractions after being purified, and also to collect and potentially recycle the electrolyte. The general schematic of an OEFFE device is illustrated in **Figure 3.1d**.

3.2 Preliminary Results

I first attempted to test OEFFE experimentally by adding the chimneys to the previously developed and optimized planar mFFE device[39]. The parts of the device were made of poly(methyl methacrylate) by robotic milling and bonded together with CH_2Cl_2. Despite the apparent simplicity of OEFFE, all of my initial attempts to construct a functional OEFFE device had failed. The flow through the separation channel was not uniform (streamlines were significantly curved) and always diverted from the separation channel into the chimneys (**Figure 3.2a**). Experimental variation of the device geometry and operation conditions proved to be a slow and inefficient way of solving this problem. In other words, milling new prototypes was not an efficient method of optimization.

3.3 Optimization of OEFFE

3.3.1 COMSOL Simulations and w/w_{tot}

Difficulties of experimental optimization of a real OEFFE device prompted me to design a virtual OEFFE device for its theoretical optimization before building a real device. The virtual OEFFE device was constructed with COMSOL Multiphysics 4.3a commercial software (COMSOL Group, Palo Alto, CA), a program which allows complete modeling of the flows within the device. The COMSOL simulation uses 3D modeling and presents the streamline patterns from a top view for clarity of demonstration. The **Material and Methods** section highlights experimental parameters, equations, meshing conditions, and boundary conditions used. To reduce computation time, only one half of the symmetrical device was simulated. It was not necessary to simulate an entire device: **Figure 3.3** illustrates a similar profile of flow streamlines when both halves are incorporated.

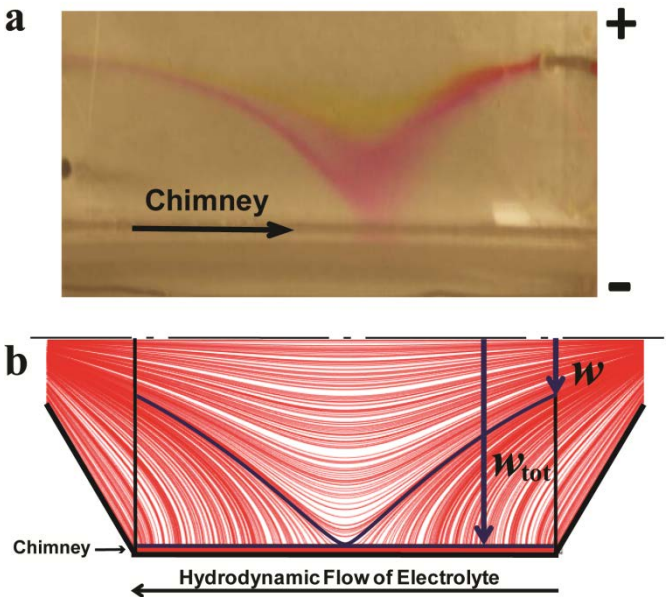

Figure 3.2: Flow non-uniformity in non-optimized OEFFE device: (a) real and (b) virtual. The hydrodynamic flow rate in both the virtual and real devices was 5 mL/min. A mixture of 2 dyes (fluorescein and rhodamine B) was continuously injected in the real device at a rate of 4 μL/min. The electric field was 50.0 V/cm. In the non-optimized device, the dye streams were deflected into the chimneys, diminishing the quality of separation. The virtual model illustrates the definition of the optimization parameter w/w_{tot} (see details in the text). Maximizing this parameter leads to a more uniform flow across the width of the separation channel. The value of w/w_{tot} in this example is 0.26 while its theoretical maximum is 1. All parts show halves of the devices.

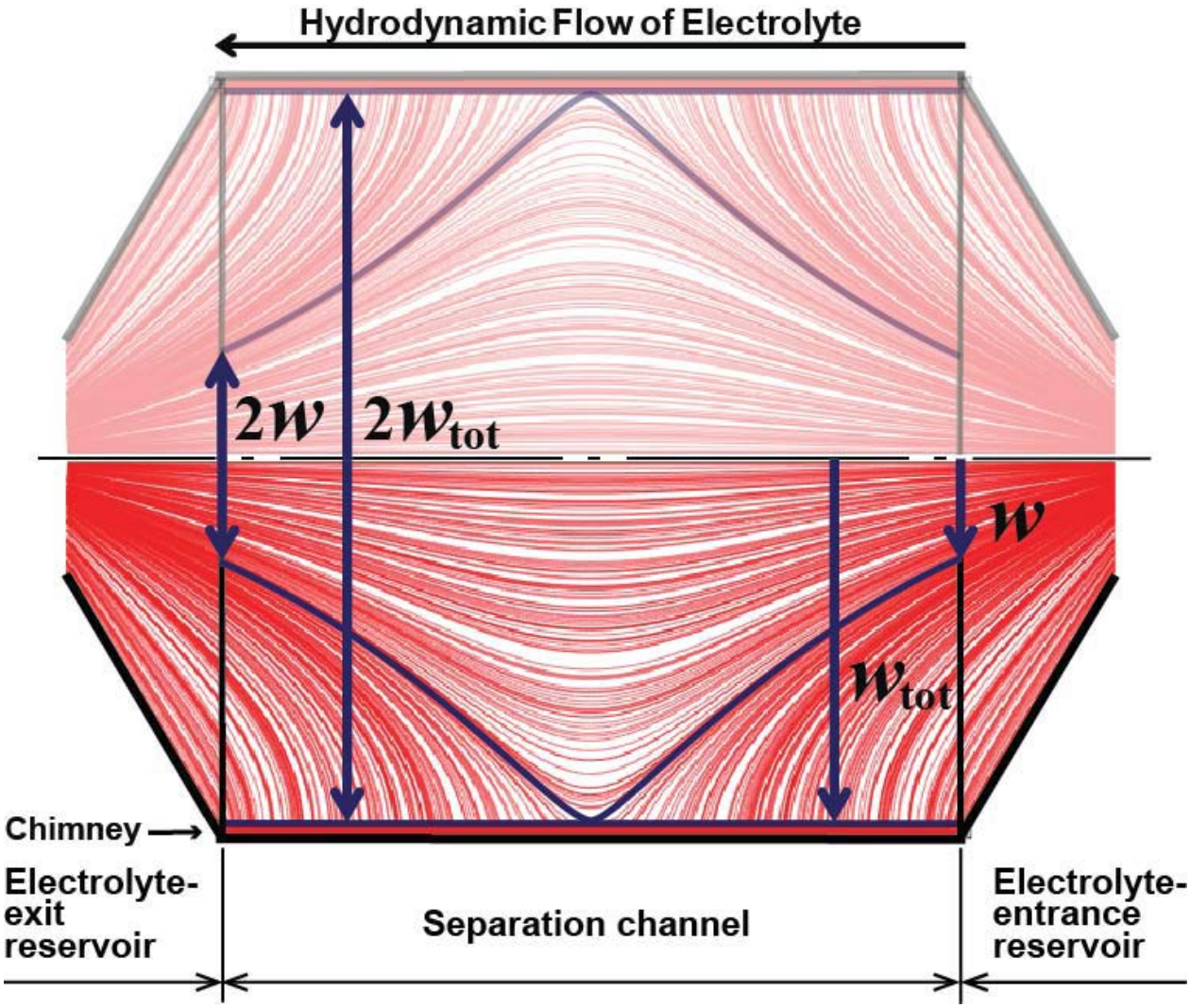

Figure 3.3: Top-view *in-silico* COMSOL simulation of hydrodynamic flow trajectories in the presence of chimneys. For conceptual clarity, the entire virtual device is illustrated. The symmetry plane is present at half of the width (w_{tot}), and for simulation performance, calculating the hydrodynamic flow streamlines is less time consuming. The semi-transparent half of the virtual device is the mirror image of that shown in the lower half with respect to geometric features and simulated streamlines. Thus, the optimization parameter (w/w_{tot}), in this case, is equal to that calculated for the entire virtual device ($2w/2w_{tot}$).

A number of virtual devices were studied, mimicking the initial experimental devices which had non-uniform flows. The flows in the virtual devices were similar to the ones in the real devices (see example in **Figure 3.2b**), which confirmed the accuracy of the virtual device operation. After this test, I could use the virtual OEFFE device for the optimization of its geometry. The goal was to achieve as uniform flow in the separation channel as possible. A numerical parameter used to characterize flow

uniformity was a ratio w/w_{tot} (see **Figure 3.2b**). Where, w is the width of the part of the separation channel entry gate which incorporates only streamlines that do not leave the main part of the separation channel and w_{tot} is the total width of the entry gate that does not include chimneys. A greater value of w/w_{tot} corresponds to a more uniform flow, and, thus, optimization was done through maximizing w/w_{tot}.

3.3.2 Optimization Parameters

3.3.2.1 Chimney Width

The first attempted parameter to optimize was the chimney width, (**Figure 3.4a**) and simulations showed that decreasing the width of the chimneys increases w/w_{tot} to a value of 0.54 when the chimney is 0.5 mm wide (**Figure 3.4b**). The limitation, however, is that the chimney width cannot be smaller than the diameter of the electrode (0.75 mm) and in reality should allow extra space for bubble escape. Therefore, the minimum chimney width was set to 1.5 mm (w/w_{tot}=0.44). This width is not sufficiently small to achieve a uniform flow (**Figure 3.4c**).

3.3.2.2 Sacrificial Channels

To further optimize flow uniformity needed a new feature in the device was needed that could significantly decrease the undesirable pressure gradient across the separation channel. I suggested that deep and narrow sacrificial channels (SacCs), parallel to the separation channel and located between the separation channel and the chimneys, could help to solve the problem (**Figure 3.5a**). Explaining the design and implementation of SacCs follows this logic: the SacC has a much larger volumetric flow rate than the separation channel, because of its greater depth, and as a result the flow within it is less likely to diverge into the chimneys. Additionally, the influence of the isobaric boundaries in the chimneys on the fluid dynamics in the separation channel can be further reduced.

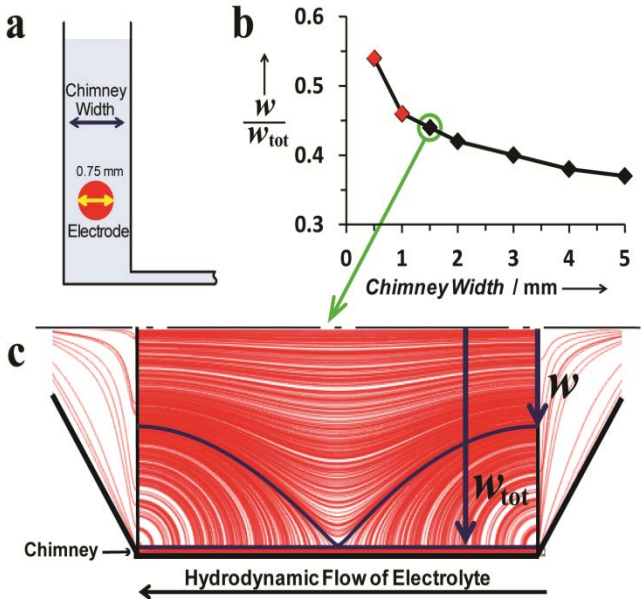

Figure 3.4: *In*-silico optimization of flow uniformity based on chimney width. **(a)** Schematic of the chimney, highlighting the chimney width in relation to the electrode width. **(b)** Dependence of flow uniformity on the width of the chimney, where (♦) identifies chimney widths that are unfeasible because of the electrode diameter being a physical limitation. **(c)** *In-silico* product of optimizing the flow by decreasing the chimney width to 1.5 mm. The resultant w/w_{tot} is equal to 0.44.

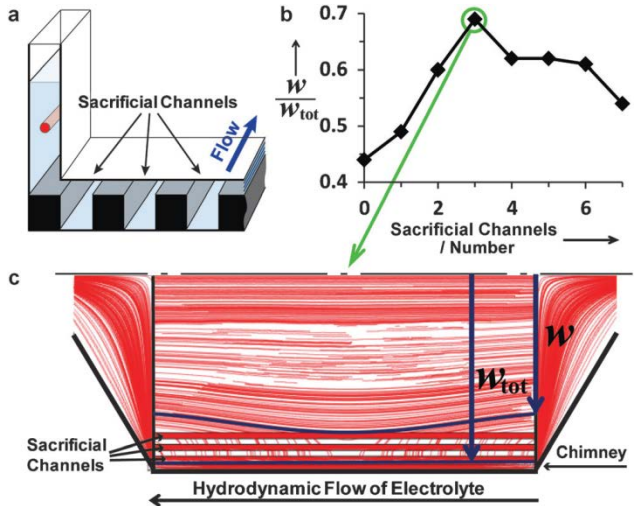

Figure 3.5: Theoretical optimization of hydrodynamic flow uniformity with respect to the number of sacrificial channels. a) Schematic of sacrificial channels built into the separation channel. b) Dependence of uniform flow on the number of sacrificial channels constructed in the separation channel. The optimal number of sacrificial channels is 3, with a w/w_{tot}=0.69. c) Improvement in flow uniformity after 3 sacrificial channels are introduced.

Next, it was decided to explore the use of multiple parallel SacCs, separated by narrow spaces, which could attenuate the fluid exchange between adjacent sacrificial channels. As a result, it was thought that SacCs could prevent the flow divergence towards the chimneys.

First a single SacC was introduced and the result was that the original hypothesis was correct—it improved flow uniformity. Then, SacC width and depth were optimized (**Figure 3.6**). As a result, both the width and depth of the SacC were limited to 1.5 mm which generated a marginal increase in the value of w/w_{tot} from 0.44 to 0.49. In an attempt to further improve flow uniformity, the effect of multiple SacCs was explored. To facilitate the faster optimization process it was assumed that: 1) all SacCs have the same dimensions and 2) the distances between them are equal. It was discovered that the dependence of w/w_{tot} on the number of SacCs displays a maximum when the number of channels was equal to 3 (**Figure 3.5b**). Three SacCs allowed w/w_{tot} = 0.69 (**Figure 3.5c**). While the width of the SacC was an important optimization parameter (**Figure 3.6a**), it became apparent that one wide channel did not have the same effect as three narrow channels (**Figure 3.7**). I also tested the final theoretical model for its robustness with respect to SacC depth (**Figure 3.8**) and hydrodynamic flow rates (**Figure 3.9**). These simulations were performed to ensure that any variability that might be caused by machining or operational precision did not significantly affect the device performance. In both cases, the optimized OEFFE proved to be robust.

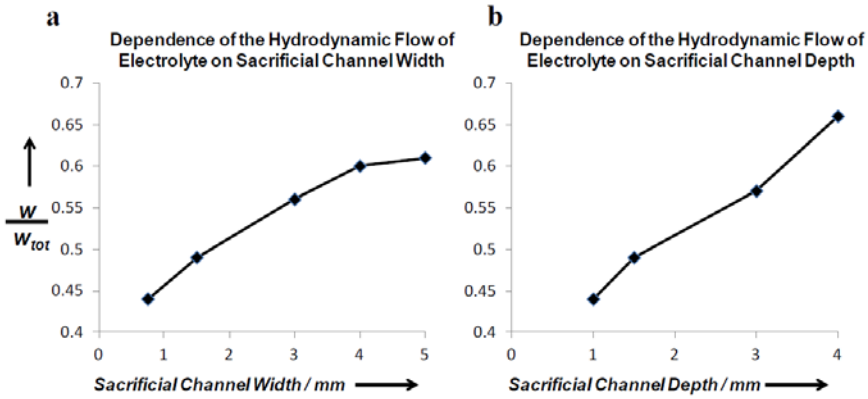

Figure 3.6. The dependence of the hydrodynamic flow uniformity on sacrificial channel dimension. (a) The width is varied when the sacrificial channel depth is set at 1.5 mm. (b) The depth is varied when the sacrificial channel width is set at 1.5 mm. Increasing the depth of the sacrificial channel had the greatest effect, however due to the tools that were available, the sacrificial channel depth was limited to 1.5 mm. With respect to the width of the sacrificial channel, larger widths provide improvement in flow uniformity. However, a width of 1.5 mm was chosen because it was prudent to consider adding further sacrificial channels before using very wide channels that would occupy more space in the separation channel. The ultimate purpose of the sacrificial channels was to improve flow uniformity by exploiting the combination of shear forces in shallow (0.200 mm) channels and inertial forces in the deeper (1.5 mm) sacrificial channels. For this, more than one sacrificial channel was needed.

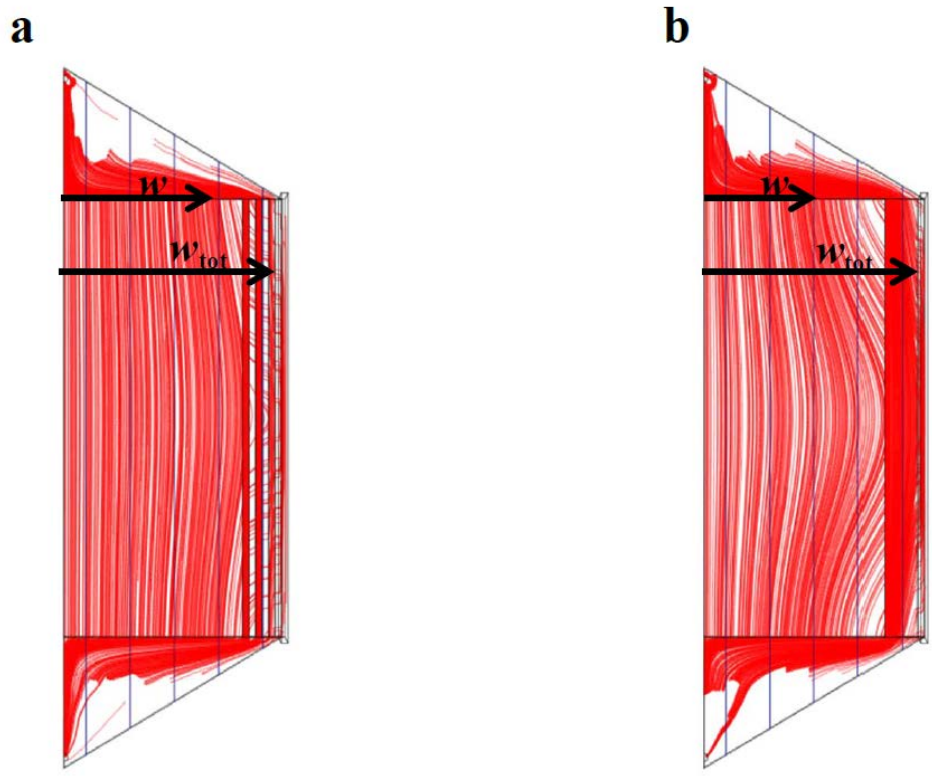

Figure 3.7: *In-silico* optimization of electrolyte flow in OEFFE by comparison of one wide sacrificial channel vs. three narrow sacrificial channels. (a) The presence of 3 narrow sacrificial channels decreases the divergence in flow compared with (b) where only 1 wide sacrificial channel is used. This is corroborated by the w/w_{tot} values of 0.69 and 0.56 for (a) and (b) respectively. This validates the greater significance of multiple sacrificial channels compared with one wide sacrificial channel.

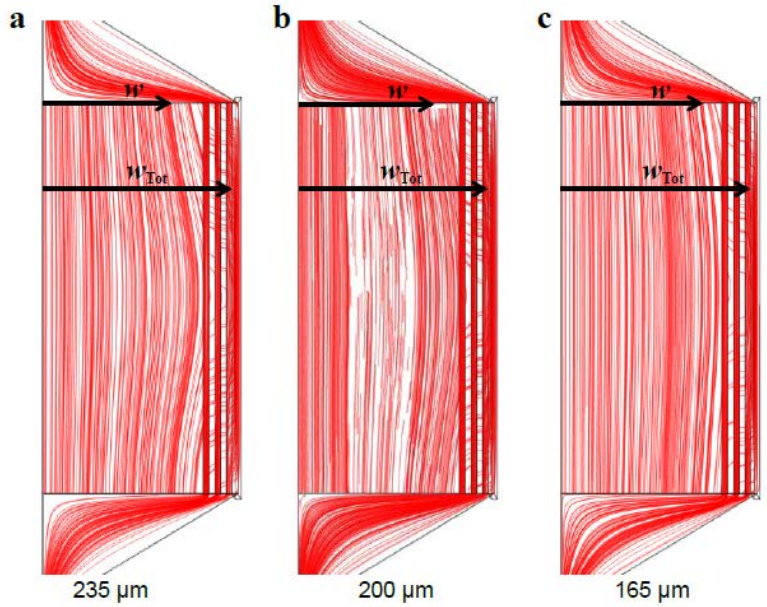

Figure 3.8: *In-silico* validation of OEFFE robustness with respect to separation channel depth. The w/w_{tot} values are 0.68, 0.69, and 0.71 for the (a) 235 µm, (b) 200µm, (c) 165 µm deep separation channels respectively. Both panels (a) and (c) illustrate two possible depths, which reflect the precision of machining when fabricating a 200 µm separation channel. The w/w_{tot} values suggest negligible influence on flow non uniformity.

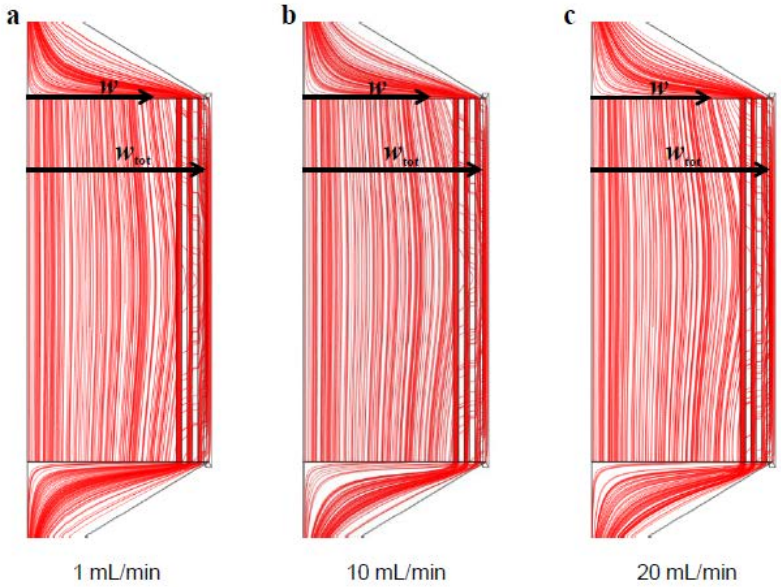

Figure 3.9: *In-silico* validation of OEFFE robustness with respect to hydrodynamic flow rate. Variations in hydrodynamic flow rates were varied from (**a**) 1 mL/min to (**b**) 10 mL/min, and (**c**) 20 mL/min to evaluate if w/w_{tot} would change drastically. In effect, all simulations demonstrate that the w/w_{tot} value is consistent across these three flow rates (w/w_{tot} = 0.69).The tested flow rate range is well beyond the flow rate error of the syringe pumps used (± 1%). It was not logical, however, to expand the flow rate range further because higher flow rates would decrease resolution, and slower flow rates would increase band broadening. Both situations would result in a decrease of separation quality.

3.4 Testing Optimized OEFFE Prototype

The hard copy of the theoretically optimized OEFFE device was then prepared using the approach described above. The device was first tested for flow uniformity. The sample flow had relatively straight streamlines suggesting that the optimization was successful, and once again proving the accuracy of the virtual device operation. Then the device was tested for bubble formation and accumulation. Bubbles formed on the electrodes and dislodged from them when they reached a critical size. Bubbles vented out into the atmosphere and did not enter the separation channel. Under such conditions the electric current showed no drift during a 12 h period of continuous work, thus, suggesting its steady-state bubble removal.

The final test was for stability of electrophoretic separation. A mixture of three dyes (rhodamine B, rhodamine 6G, and fluorescein) was continuously injected by a syringe pump that provided uninterrupted injection for 12 h. The stability of separation was judged by the steadiness of the three streamlines. No deterioration in separation quality was noticed (**Figure 3.10**), suggesting the steady-state operation of the device. On the other hand, only negligible widening of streamlines during their passage through the separation channel suggests minimal contribution from multiple sources of band-broadening

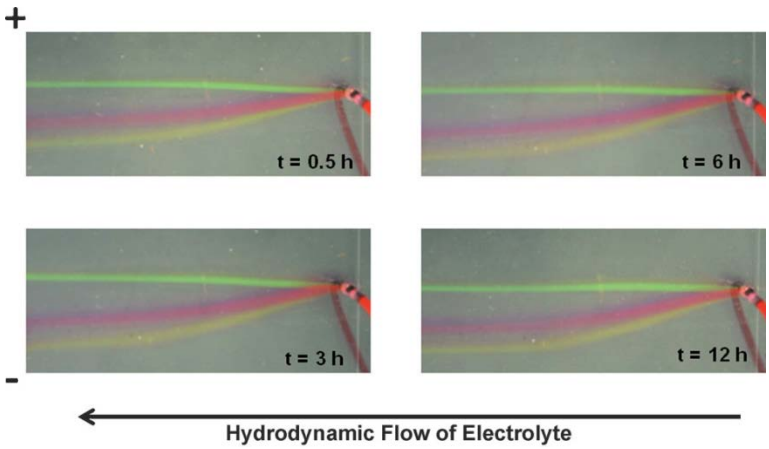

Figure 3.10: Steady-state continuous separation of 250 µM fluorescein (green), 250 µM rhodamine B (pink), and 250 µM rhodamine 6G (yellow) by OEFFE. An electric field of 50.0 V/cm was applied across the chip for a 12 h period. The hydrodynamic flow rate of the electrolyte was (5.00 ± 0.5) mL/min. A mixture of the three dyes was introduced at a flow rate of (4.00 ± 0.01) µL/min. Current reading was stable at (25 ± 1) mA. Removing the bubbles from the OEFFE device prevented electric field distortion and supported its steady-state separation with constant quality of separation.

such as diffusion, injection bandwidth, convection, and hydrodynamic broadening. Injection bandwidth is limited by simply decreasing the diameter of the sample inlet. Decreasing the depth of the separation channel reduces convective and hydrodynamic broadening. Therefore, not only can this device support steady-state continuous separation, but it also satisfies the general requirement of negligible band broadening.

3.5 Concluding Remarks

To conclude, OEFFE has successfully demonstrated steady-state small-scale continuous separation. OEFFE ultimately solves the problem of the deterioration of separation quality over time by preventing the accumulation of bubbles in the device. The introduction of chimneys caused non-uniformity in hydrodynamic flow, which was circumvented by novel features called SacCs. With the assistance of COMSOL simulations, the appropriate geometries of the chimneys and SacCs were optimized to achieve acceptable flow uniformity. According to the present results, flow uniformity can be further optimized and will be evaluated in future studies. Although only an OEFFE prototype was fabricated in plastic, it will be prudent to create analogues in solvent resistant material, to expand the scope of solvents and analytes for which OEFFE is suitable. It should be noted that classical electrophoresis is applicable for separation of analytes with different charge/size ratios. Modifications of classical electrophoresis have been developed for the separation of uncharged species. Micellar electrokinetic chromatography uses charged surfactants, at concentrations that are greater than critical micelle concentration, to separate uncharged species with different hydrophobicities[73-75]. Dielectrophoresis, another example, uses non-uniform electric fields to separate uncharged species with different dipole moments[76,77]. Both of these techniques will be discussed in greater detail in **Chapter 5**. Achieving steady-state continuous separation, with a technologically simple solution, will stimulate efforts aiming at practical integration of CFS with CFP.

3.6 Materials and Methods

3.6.1 COMSOL Simulations

Simulation of OEFFE devices was achieved used COMSOL. The steady state Navier-Stokes equation was used for the computations, with the condition of non-compressible flow. The laminar flow physics model was chosen and input a flow rate of 5 mL/min was introduced into the electrolyte inlet (shown in **Figure 3.11**). The boundary conditions include: no-slip walls; laminar inflow at the inlet; and no viscous stress at the outlet. The meshing geometry used was tetrahedral, with a fine size in areas of large volume (exit and entrance reservoirs), and extremely fine geometry in narrow regions (separation channel, sacrificial channels, and chimneys). Default stabilization conditions (with a tuning parameter Ck = 1) were selected: streamline diffusion and crosswind diffusion. 3D models were prepared to fully capture the flow system in only one half of the device to facilitate simulation time. The mathematical model includes the following relations.

Laminar flow equations inside the device:

$$\rho(v\nabla)v = \nabla\{-pI + \mu[\nabla v + (\nabla v)^T]\} \quad \textbf{(3.1)}$$

$$\rho\nabla v = 0 \quad \textbf{(3.2)}$$

Wall boundary condition:

$$v = 0 \quad \textbf{(3.3)}$$

Inlet condition:

$$L_{enter}\nabla_t\{-p_{enter}I + \mu[\nabla_t v + (\nabla_t v)^T]\} = -p_{enter}n \quad \textbf{(3.4)}$$

$$\nabla_t v = 0 \quad \textbf{(3.5)}$$

Outlet condition:

$$p = p_0, \ \ [\mu(\nabla v + (\nabla v)^T)]n = 0 \quad \textbf{(3.6)}$$

Symmetry conditions at the symmetry plane $x = 0$

$$vn = 0, \quad K - (Kn)n = 0 \tag{3.7}$$

$$K = [\mu(\nabla v + (\nabla v)^T)]n \tag{3.8}$$

Where, ρ and μ are density and viscosity of the liquid; v and p are the velocity and pressure; K is the viscous force at the symmetry plane; p_{enter} and p_0 are the pressures at the inlet and outlet, respectively; L_{enter} is a parameter used by COMSOL in the inlet condition, I is the unit tensor; n is the normal to the walls or to the symmetry plane; the superscript T denotes a transpose matrix.

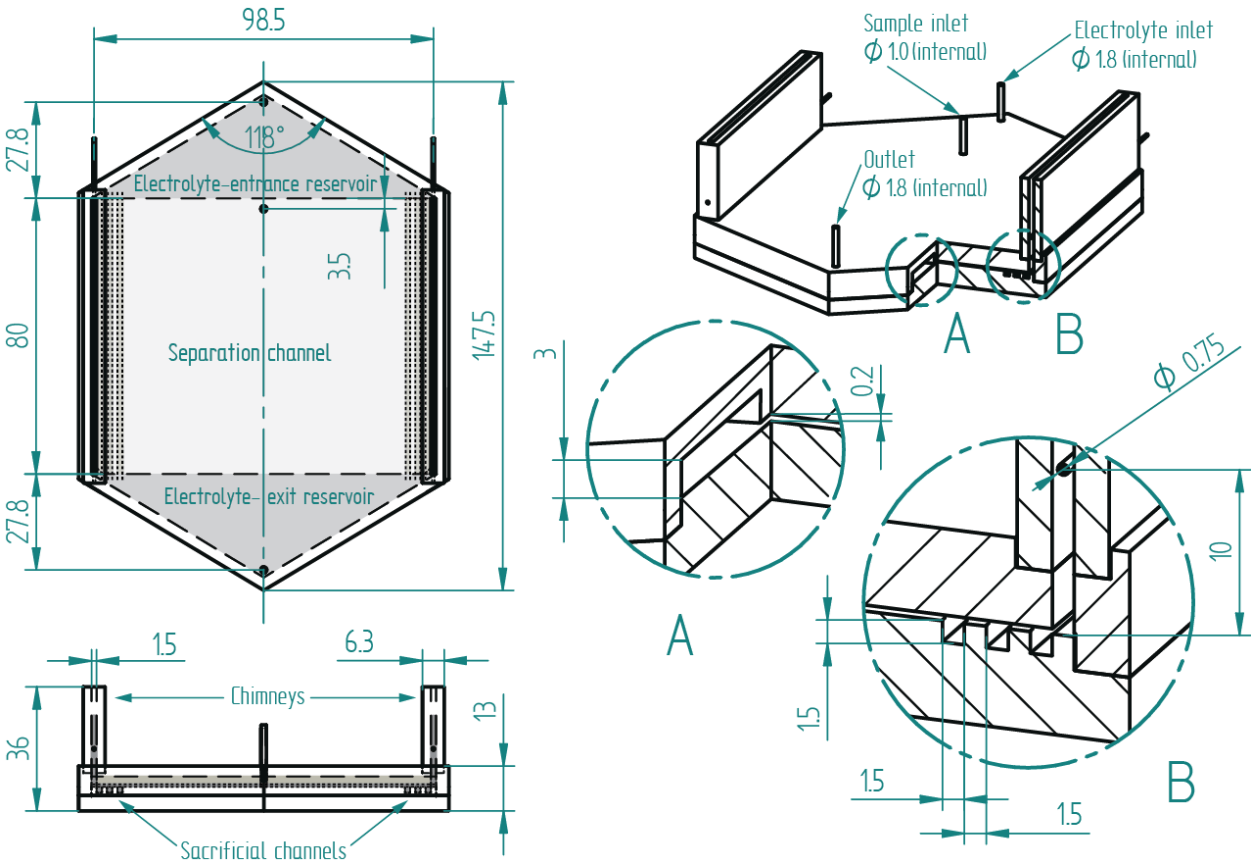

Figure 3.11: Schematic representation of an assembled OEFFE device. All units are in mm. This model differs from that illustrated in **Fig. 3.1d** by omitting sample outlets in the separation channel. The purpose of this work was to demonstrate successful bubble removal, and steady-state continuous electrophoretic purification. Therefore, for simplicity of the experiment, a common output for electrolyte and products was used.

3.6.2 Reagents

All reagents were purchased from Sigma Aldrich, unless otherwise mentioned. OEFFE prototypes were fabricated from poly(-methyl methacrylate) stock material using a MDX-540 robotic milling machine. The optimized cutting speeds for the end mills have already been described in full detail in **Chapter 2**. An electrolyte solution was prepared with 25 mM 4-(2-hydroxyethyl)-1-piperazineethanesulfonic acid (HEPES) (99.5%) and was adjusted with 10m NaOH to pH 7.5. Triton X-100 (0.01% [w/v]) was added to it and the mixture was deoxygenated by bubbling with N_2 overnight. A sample containing 250 µM of each fluorescein, rhodamine B, and rhodamine 6G, was prepared in this electrolyte. A separate 10% EtOH solution was used as a primary wash solution to wet the surface of the OEFFE device. All solutions were prepared using de-ionized H_2O.

3.6.3 OEFFE Fabrication

The stock material used was PMMA (Johnston Industrial Plastics, Toronto, Canada), and was cut using a series of end mill tools to accurately and precisely shape the prototypes. The optimized cutting speeds for the end mills have already been described in full detail in **Chapter 2**. Fabrication of OEFFE involves milling bottom, top, and chimney substrates. The three substrates are then bonded together using small volumes of CH_2Cl_2. CH_2Cl_2 was injected carefully to provide a tight seal at the edges of the device. The device was clamped together for 10 minutes to allow the solvent to completely perfuse and dry at the edges. Platinum electrodes (100 mm long and 0.75 mm in diameter) were installed into the chimneys and connected with insulated copper wires to a power source. The power source used was a high-voltage Electrophoresis Power Supply EPS 3501 XL (Amersham Pharmacia Biotech, New Jersey, USA). The completed device, with the appropriate dimensions, can be found in **Figure 3.11**.

3.6.4 OEFFE Experiment

The hydrodynamic flow of the electrolyte was driven by a continuous flow syringe pump system (New Era Pump System Inc, Farmingdale, NY, USA). The electrolyte flow rate in the experiment highlighted herein (5.00 ± 0.05) mL/min. A separate syringe pump (Harvard Apparatus Pump II, Saint-Laurent, Canada) was used to introduce the sample at a flow rate of (4.00 ± 0.01) µL/min. Experiments were carried out at room temperature. The OEFFE device was placed on top of metal blocks, which were in contact with ice packs, to help prevent overheating.

Before using the device, it was placed into the oven over night at 65ºC. This was to ensure that the plastic was not wet. The wet surface caused the device to swell and clog the channels. The OEFFE device was allowed to cool to room temperature after removal from the oven. A 10% EtOH solution was passed through the device to wet the entire surface prior to the electrolyte. The electrolyte was then introduced along with the sample at the prescribed flow rates mentioned above. The voltage applied to the system was 500 V, which represents an electric field strength of 50.0 V/cm inside the separation channel. For 12 hours, the current was recorded and digital pictures (Nikon 7000) were taken to monitor the sample separation quality in the presence of an electric field. Bubbles were successfully detached from the surface of the electrodes, but an occasional mechanical shock was added to the chimneys to aid in detachment. After the device was used, it was flushed with de-ionized H_2O to wash out any remaining electrolyte and placed back in the oven to dry overnight at 65ºC.

CHAPTER 4: REDUCING pH GRADIENTS IN FREE-FLOW ELECTROPHORESIS

The presented material was published previously. Adapted with permission from:
Agostino, F.J.; Cherney, L.T.; Kanoatov, M.; and Krylov, S.N. Reducing pH Gradients in Free-Flow Electrophoresis, *Analytical Chemistry*, **2014**, 86, 5656-5660.

Contributions to the article: fabricated all mFFE devices, designed all experiments, assisted in all experiments, first author of the manuscript, and prepared all figures.

4.1 Introduction

Milli-scale free-flow electrophoresis (mFFE) is a promising continuous-flow purification technique that is well suited for integration with small-volume CFS. The purification stability of mFFE, however, needs to be significantly improved before it can be feasible for this combination. One of the major sources of instability of mFFE is attributed to the ions produced as a result of electrolysis. These ions can form pH and conductivity gradients in mFFE, which are detrimental to separation quality. The severity of these gradients has not been thoroughly studied in mFFE.

The electrolytic ions, H^+ and OH^-, pose a problem because of their migration from the electrodes into the separation channel, where they can potentially alter the pH and conductivity of the electrolyte. Such pH gradients are undesirable when analyzing pH-sensitive species. pH gradients can affect the analytes by altering their structural conformation, reactivity, and optical properties (which can render the analytes undetectable). In addition, the establishment of pH and conductivity gradients may diminish FFE separation quality by altering sample stream trajectories and causing band broadening[78]. In the macro-FFE format (mL to L/min flow rates), the adverse effects of pH gradients on separation efficiency have been observed, studied, and alleviated by introduction of ion-impermeable membranes[79].

The use of membranes, however, always reduced the effective electric field strengths in FFE experiments, and, thus, decreased their electrophoretic resolution efficiency[71,80,81]. The pH gradients in the

micro-FFE format (nL to μL/min flow rates) have only been studied in the context of ampholyte distribution in iso-electric focusing[82]. Furthermore, both the macro- and micro-FFE formats operate at flow rates that are difficult to adapt to small-volume CFS. The previous study, in **Chapter 2**, suggested that flow rates used in small-volume CFS are best-matched with the milli-FFE format (mFFE) which operates with a μL to mL/min flow rate range[39]. To date, pH gradients in mFFE have not been studied.

In this project, it was experimentally demonstrated that pH gradients do occur in mFFE devices. These results defined a set of conditions at which pH gradients become significant. It was hypothesized that the ions can be rapidly and effectively washed away, at the electrode, before causing pH gradients. The geometry of channels, within the mFFE device, were optimized to attain the necessary flow rates. Any influence that these channels might have on the hydrodynamic flow was investigated by modeling the flow profiles in a virtual device. Lastly, the effectiveness of the virtual solution was confirmed with a fabricated device.

4.2 Redefining a mFFE Device

A mFFE device (**Figure 4.1**) consists of a wide separation channel (SC) with wire electrodes, on opposite sides, which span its entire length. The buffer enters the SC as a uniform hydrodynamic flow and carries a sample mixture, which is introduced downstream of the buffer entry. As a sample mixture travels through the applied electric field, it is resolved into individual component streams, which are defined by their respective electrophoretic mobilities. Electrophoretic conditions are chosen to maximize the separation between component streams and to direct them toward a row of collection outlets. The distance between the terminal outlets, anode outlet (AO) and cathode outlet (CO), is defined as the separation zone (SZ). The space between each of the terminal outlets and the corresponding electrode is defined as a sacrificial zone (SacZ). The two SacZs serve the purpose of dissipating any boundary phenomena that

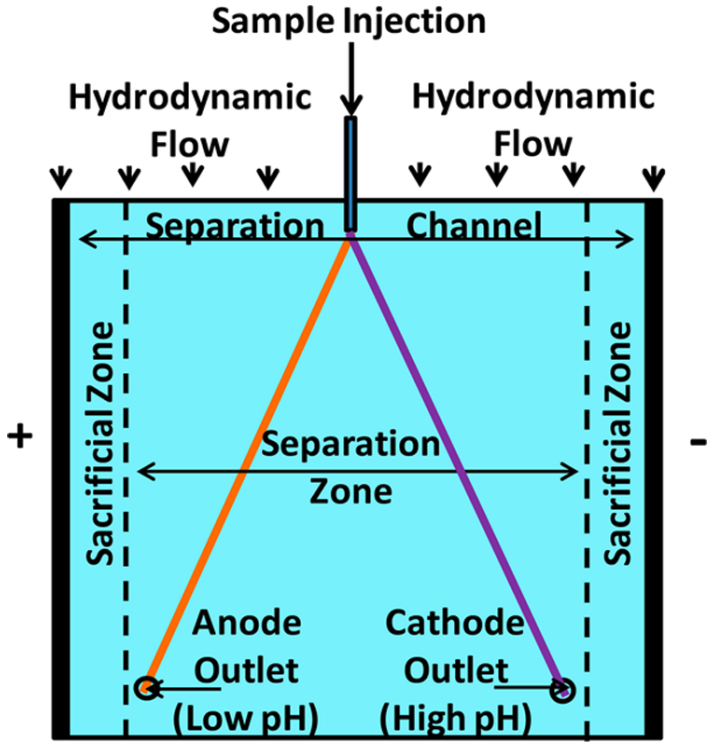

Figure 4.1: Conceptual illustration of a mFFE device. A sample mixture is carried by a uniform hydrodynamic flow and is electrophoretically separated into a negatively charged analyte stream (orange) and a positively charged analyte stream (purple). In the case of maximum sample separation, the streams are directed toward the terminal collection outlets, anode outlet (AO) and cathode outlet (CO), which define the boundaries between the separation zone (SZ) and the sacrificial zones (SacZ). The SZ area is allocated for unperturbed sample separation while the SacZ areas serve to dissipate the effects of boundary phenomena (i.e., flow perturbation). The difference between buffer pH at AO and CO defines the ΔpH parameter.

occur at the edges of the SC, such as flow perturbation and bubble generation. In this case, each SacZ area is 10% of the total SC area.

4.3 Forming pH Gradients in mFFE and the ΔpH Parameter

H^+ and OH^-, generated at the anode and cathode, respectively, migrate toward the interior of the SC, forming pH and conductivity gradients. The extent to which these gradients permeate the SC depends on the applied electric field strength, buffer concentration, and hydrodynamic flow rate. To avoid any negative effect associated with pH gradients, it is important to ensure that they do not extend into the SZ. The existence of pH gradients in the SacZ areas, however, is inconsequential to mFFE separation efficiency, because the maximum separation distance between two analytes is limited by the distance

between the terminal outlets. By determining the difference in pH at the AO and the CO, I define a parameter, $\Delta pH = pH_{CO} - pH_{AO}$, which reflects the capacity of pH gradients to influence the separation efficiency of the device. Conceptually, a ΔpH equal to 0 indicates a situation in which existing pH gradients do not extend into the SZ. Thus, the goal of pH gradient optimization is to minimize ΔpH.

4.4 Achieving Reduction in pH Gradients

The minimization of ΔpH can be achieved by increasing the buffer concentration, reducing the electric field strength, or increasing the hydrodynamic flow rate. Typically, the buffer concentration is limited by the highest value at which electrolyte overheating does not occur. In this case, the buffer concentration was limited to 25 mM to prevent boiling of the electrolyte. Both the flow rate and the electric field strength are tuned to obtain desired sample resolution. I was interested to determine the magnitudes of ΔpH when typical mFFE flow rates and electric field strengths are used. mFFE devices have the capacity to reach flow rates as low as 1 mL/min without significant band broadening and electric field strengths of 100 V/cm without overheating. The range of investigated flow rates and electric field strengths were 1−8 mL/min and 25−100 V/ cm, respectively. It was observed that a significant increase in ΔpH occurs as flow rates decrease and as electric field strengths increase. Combinations of smaller flow rates with higher electric field strengths further increase ΔpH. It is important to recognize that the conditions which cause the highest ΔpH values (low flow rates and high electric field strengths) also represent conditions that maximize the electrophoretic separation. pH gradients that permeate the SZ, thus, prevent mFFE from reaching its full potential in terms of separation efficiency. It is desirable, therefore, to minimize ΔpH while allowing the usage of separation conditions that are most advantageous. This problem can be addressed by implementing modifications to the mFFE device geometry, in particular the geometry of the SacZ areas.

4.5 Using Deep Channels and the Versatility of Sacrificial Channels

Increasing the depth of the SacZ areas can increase the flow rate within them, without increasing the flow rate in SZ. Deep channels were originally implemented to rapidly remove electrolytic bubbles[64]. The same logic can be applied to remove electrolytic ions. It is possible to calculate the migration time of H^+ and OH^- across the SacZ, since this time is proportional to their electrophoretic mobility. The assumption can be made that the conductivity in the SacZ areas will increase due to the influx of H^+ and OH^- and that this will have a negative effect on both electric field strength and the electrophoretic velocity. Therefore, the minimum migration time will be proportional to the voltage supplied by the power supply. From this information, it is possible to determine the necessary linear flow velocity to evacuate H^+ and OH^- before their migration into the SZ area. In the mFFE device, H^+ was used as the model since it has the highest electrophoretic mobility (3.6×10^{-7} $m^2/(V \cdot s)$)[83]. With this knowledge, it was determined that H^+ ions would have to be evacuated from the SacZ within 3 s, in the presence of an 100 V/cm electric field, before migrating into the SZ (see **Section 4.8.2**). For H^+ ions to be evacuated in less than 3 s, the linear flow velocity within the SacZ would have to be at least 3.3×10^{-2} m/s. This can be achieved, with a buffer flow rate of 1 mL/min, if the depth of the SacZ is increased to 2.4 mm, or 12 times the depth of the SZ. High flow rates in the SacZ areas, however, can affect flow uniformity within the SZ. In an effort to investigate any influence that deep SacZ areas might have on the hydrodynamic flow profiles in the SZ, the flow streamlines were modelled in a virtual device using COMSOL. It was found that the flow within the SZ does deviate toward the SacZ areas (**Figure 4.2 top**). In **Chapter 3** I previously defined a quantitative parameter that described flow uniformity in a FFE device. Flow uniformity is characterized by the ratio of w/w_{tot}, where w is the width of the SZ entry gate which incorporates streamlines of flow that do not enter the SacZ and w_{tot} is the total width of the SZ. Ideally, a w/w_{tot} should be equal to 1. It is important to note that the current definition of w_{tot} is different than what was reported in **Chapter 3**. Formerly, w_{tot} incorporated the entire SC. However, since the SacZs are not

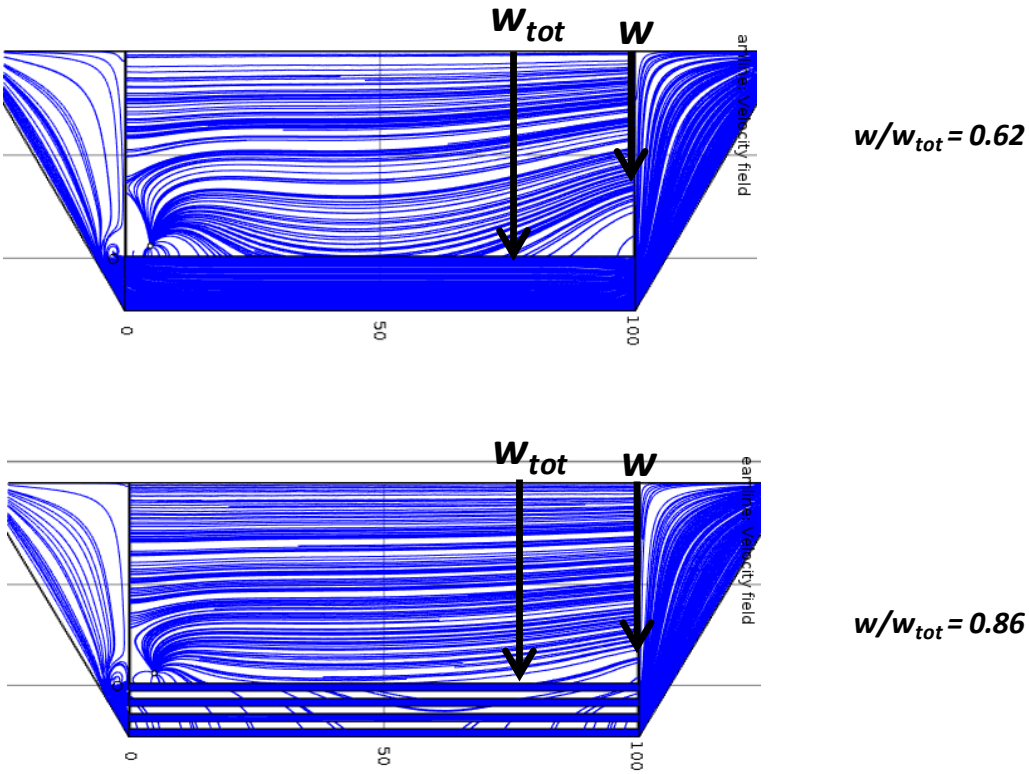

Figure 4.2: COMSOL simulation of buffer flow showing the top-view of a mFFE device. Only one half of the virtual model is illustrated. In both devices, the flow is 8 mL/min. In the top panel the depth of the SacZ area is 2.4 mm, this causes flow-non uniformity to exist in the SZ. Flow uniformity is characterized by the ratio of w/w_{tot}, where w is the width of the SZ entry gate which incorporates streamlines of flow that do not enter the SacZ and w_{tot} is the total width of the SZ. Ideally, a w/w_{tot} should be equal to 1. In the top panel the resultant w/w_{tot} = 0.62. In the bottom panel, sacrificial channels are introduced. The depth of the deep channels is 3.5 mm in order to remove electrolytic ions before their migration into the SZ, but the shallow channels remain 0.2 mm deep. Flow uniformity is improved which is indicated by the increased value of the w/w_{tot} = 0.86.

used in separation, they should be excluded from w_{tot}. Therefore, from this point forward, all w_{tot} values will only include the SZ. In the virtual mFFE device, w/w_{tot} was calculated to be 0.62 (**Figure 4.2 top**). Previously, I have developed a strategy to alleviate such flow non-uniformity using sacrificial channels (SacCs).

SacCs are geometric features that can increases flow uniformity in mFFE devices. These features consist of a series of deep and shallow channels with alternating fast and slow flow rates, where inertial forces dominate within the deep channels and shear forces dominate within the shallow channels. The interplay between these two forces prevents the fluid from diverging from its original trajectories. It has already been demonstrated that SacCs can reduce flow non-uniformity in a similar mFFE device[84]. In the

new device prototype, the number of SacCs was maximized to attain the best possible reduction in pH gradients and increase of flow uniformity. The specifications of a milling machine, used for device fabrication, limited the device to a maximum of 4 sacrificial channels within the SZ. In the device setup highlighted in **Figure 4.1**, SacC depth was optimized (3.5 mm) to evacuate the ions in a similar time frame as when a single deep channel was used. The integration of 4 sacrificial channels resulted in an increase of w/w_{tot} to 0.86 (**Figure 4.2b bottom**). It should be noted that the integration of sacrificial channels does not change the distance between the terminal outlets and, thus, does not reduce the maximum resolving power of the device. Previously, it was determined that similar sacrificial channels in OEFFE did not influence the quality of separation, and it is not expected that the separation will be adversely affected here (**Figure 4.3)**.

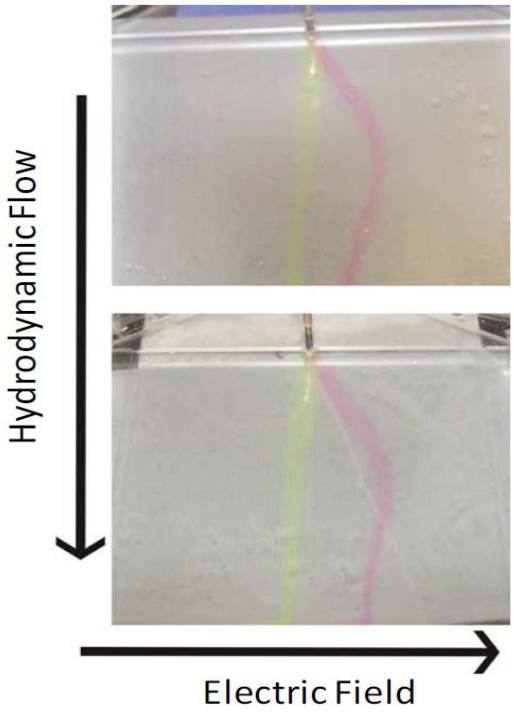

Figure 4.3: The separation of fluorescein and rhodamine B in a OEFFE device. Here, the two dyes are separated using a device without sacrificial channels (top) and with sacrificial channels (bottom). It was demonstrated that the presence of sacrificial channels has no negative influence on separation quality. The hydrodynamic flow rate is 8 mL/min and the sample flow rate is 5 μL/min, and the electric field strength is 50 V/cm.

4.6 Results

I have demonstrated the effectiveness of the modified design by implementing it into a real mFFE prototype. The device was fabricated as described in **Chapter 2**, and experiments, similar to those described in **Section 4.4**, were performed. A significant decrease in ΔpH was observed over the entire range of conditions (**Figure 4.4**), which implies that the developed solution was effective in minimizing pH gradients across the SZ. In fact, negligible changes in ΔpH were observed when all flow rates were applied up to an electric field strength of 55 V/cm. The same improvement was observed for 70 V/cm at

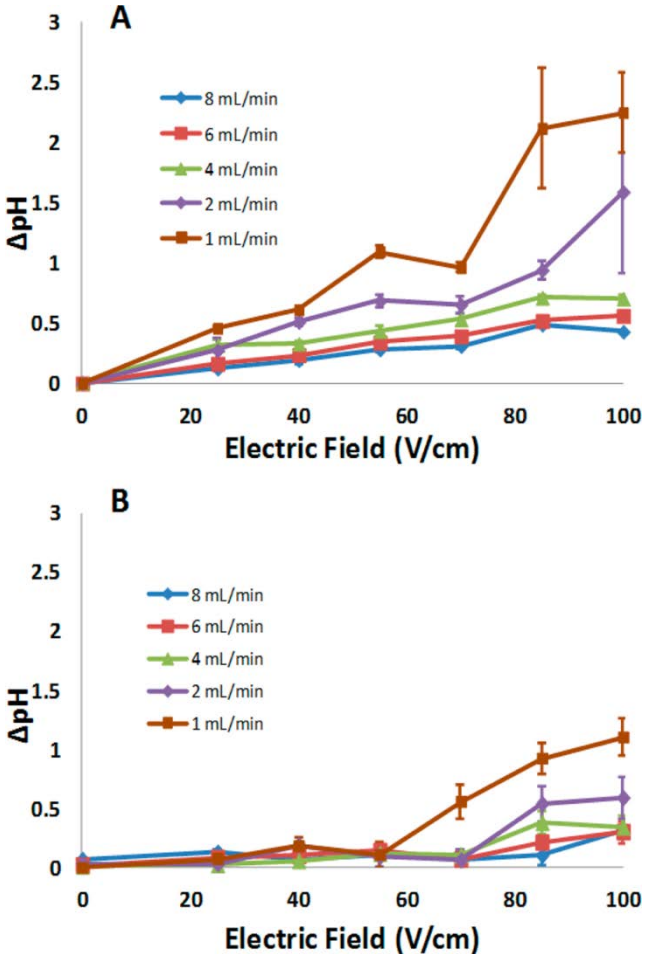

Figure 4.4. ΔpH between the anode outlet and cathode outlet of a mFFE device without (a) and with (b) sacrificial channels. H^+ and OH^- migrate across the separation channel and change the pH, thus affecting the separation conditions. Naturally, this effect worsens at higher electric field strengths and lower flow rates. Sacrificial channels, integrated in the SacZ areas, provide a region of faster flow that can evacuate H^+ and OH^- more efficiently and limit the change in ΔpH. mFFE devices with sacrificial channels can decrease ΔpH further than devices without sacrificial channels and maintain a uniform pH over a broader range of separation conditions. Error bars represent the standard deviation of three separate pH measurements at each outlet.

all flow rates except 1 mL/min. Bubbles did not pose a problem to the stability of the electric field because they were also evacuated rapidly by high flow rates within the sacrificial channels. Furthermore, it was observed that the electric current was not affected by the presence of sacrificial channels in the SacZ. This suggests that the proposed solution reduces ΔpH, over a wider range of experimental conditions, and does so without compromising the electric field strength, unlike ion-exchange membranes. These findings allow mFFE to be used at its full potential.

4.7 Conclusions

For the first time, it was demonstrated that electrolytic ions contribute to the formation of significant pH gradients in mFFE. To reduce these pH gradients, an optimization strategy was developed in which mFFE device geometry was modified. I hypothesized that increasing the flow rate in the SacZ areas would evacuate the ions and they would be unable to enter into the SZ, thereby, mitigating pH gradients. In an optimized mFFE prototype, deep and wide SacZ areas were integrated and it was observed that pH gradients were minimized, even at low flow rates and high electric field strengths. mFFE can now be used over a broader range of experimental conditions, making this technique a more feasible complement to small-volume CFS.

4.8 Materials and Methods

4.8.1 COMSOL Simulations

To simulate and study flow profiles in mFFE devices, I used COMSOL Multiphysics software version 4.3b. A virtual 3D model of the separation channel was created using discrete geometry. The 3D results are illustrated in a 2D format for ease of visualizing the flow profiles. A steady state virtual system was designed using the Laminar Flow module. Conditions and settings for the simulations have been described previously in **Chapter 3**.

4.8.2 Calculating the Necessary Depth of SacCs for H^+ Evacuation

Electrophoretic mobility of H^+: 3.6×10^{-7} $m^2/(Vs)$

Electric field strength: 100 V/m

Therefore the electrophoretic velocity of H^+:

$$\left(3.6 \times 10^{-7} \frac{\mathrm{m}^2}{\mathrm{V} \cdot \mathrm{s}}\right)(10^4) = 3.6 \times 10^{-3} \frac{\mathrm{m}}{\mathrm{s}} \quad \textbf{(4.1)}$$

Width of the Sacrificial Zone (SZ): 0.001 m

Time for H^+ to travel across the SZ width:

$$\frac{0.010 \text{ m}}{3.6 \times 10^{-3} \frac{\mathrm{m}}{\mathrm{s}}} \sim 3 \text{ s} \quad \textbf{(4.2)}$$

Therefore, the flow within the SZ needs to be fast enough to evacuate H^+ in less than 3 s.

Length of SZ: 0.08 m

Flow velocity necessary within SZ:

$$\frac{0.10 \text{ m}}{3 \text{ s}} = 0.033 \frac{\mathrm{m}}{\mathrm{s}} \quad \textbf{(4.3)}$$

Hagen-Poisuelle equation was re-arranged to approximate the channel height necessary to provide the required velocity of 0.033 m/s

$$H = \sqrt{\frac{12\ v\eta L}{\Delta P}} = \sqrt{\frac{12(0.033 \text{ m} \cdot \text{s}^{-1})(0.001 \text{ Pa} \cdot \text{s})(0.08 \text{ m})}{5.5 \text{ Pa}}} \quad \textbf{(4.4)}$$

Where v is the fluid velocity, L is the length of the channel, P is the pressure, and η is electrolyte viscosity. ΔP is calculated from COMSOL as the pressure difference from the entry and exit of the SC.

4.8.3 Reagents

All reagents were purchased from Sigma-Aldrich, unless otherwise stated. A 25 mM 4-(2-hydroxyethyl)-1-piperazine-ethanesulfonic acid (HEPES, 99.5% purity) buffer solution with Triton X-100 (0.01% [w/v]) was adjusted to pH 7 with 10 M NaOH and used in all experiments. The buffer mixture was deoxygenated by overnight N_2 bubbling. A separate 10% EtOH solution was used as a primary wash solution to wet the surfaces of the mFFE devices. All solutions were prepared using deionized H2O (EMD Millipore, Mississauga, Canada), the electrical resistivity of which was 18.2 MΩ•cm. The hydrodynamic flow of the buffer was driven by a continuous flow syringe pump system (New Era Pump System Inc., Farmingdale, NY, USA). The power source used was a high-voltage Electrophoresis Power Supply EPS 3501 XL (Amersham Pharmacia Biotech, New Jersey, USA).

4.8.4 mFFE Device Operation

The fabrication of mFFE devices is described in **Chapter 2**. The buffer flow rates ranged from 1.00 ± 0.05 to 8.00 ± 0.05 mL/min. The electric field strengths used ranged from 25 to 100 V/cm inside the separation channel. Experiments were carried out at room temperature. The mFFE devices were placed on top of metal blocks, which were in contact with ice packs, to prevent overheating. Buffer elution fractions were collected from two outlets, and their pH was measured using the Orion benchtop pH/mV/temperature/ion meter model 710A (ThermoFisher Scientific, Waltham, MA, USA).

CHAPTER 5: IMPROVING RESOLUTION USING NON-ORTHOGONAL-TO-THE-FLOW FREE-FLOW-ELECTROPHORESIS (NOFFE)

5.1 Introduction

Until now, I have addressed two major issues that can destabilize steady-state purification in a mFFE device: bubble accumulation and pH gradients. In addition to steady-state purification, I will discuss two other important limitations that need to be addressed before considering the integration of FFE into CFC. The first limitation is the inability of standard modes of electrophoresis to separate many of the potential target molecules, such as pharmaceuticals, which are either difficult to dissolve in aqueous solutions or are neutral. The other limitation is the inadequate resolving power of FFE (with the exception of FFIEF) when compared to existing discontinuous purification techniques.). It will be necessary to improve the resolution quality typically associated with FFE in order to fully complement microreactors. Often, components of a reaction mixture have very similar electrophoretic mobilities; thus making their separation very difficult. In the next sections I will discuss the need to develop suitable FFE technology that is capable of purifying the components of samples that are typically not suited for electrophoretic separations.

5.1.1 Organic and Neutral Molecules

Water soluble organic dyes, similar to those used as model systems through this dissertation, are widely used as tracer molecules and model analytes for proof of concept experiments. Beyond these, however, there has been very little work performed on the separation of organic molecules using FFE. Organic solutes are difficult to separate by electrophoresis for obvious reasons: (i) reduced solubility; (ii) abundance of neutral species; and (iii) lack of compatible organic electrolytes for FFE. Yang et al.

experimented with diluting the electrolyte in a water/methanol mixture to increase the solubility of organic solutes. As a result, they were able to purify organic solutes that have low aqueous solubility[85].

In general, electrophoresis is incompatible with organic solvents used in most chemical syntheses: it is difficult to solubilize electrolytes and generate electric fields. Modern synthetic approaches, however, are being developed to minimize the use of organic solvents[86]. There are even micro-reactors that avoid organic solvents and perform chemical transformations at high temperatures and high pressures in aqueous solvents[87]. Ionic liquids are also being investigated as potential replacements for organic solvents[88,89]. In general, a shift from organic liquids would facilitate the use of electrophoresis as a purification approach. At the rate of synthetic development, it would seem more likely for organic syntheses to adopt green alternatives before electrophoresis purification is made suitable for organic solvents. Until then, there are three potential purification approaches that are compatible with FFE, and each one will be discussed here.

5.1.1.1 Micellar Electrokinectic Chromatography

Miceller electrokinetic chromatography (MEKC) in the FFE format is a potential solution to separate neutral and hydrophobic molecules. MEKC is typically used in capillaries as a discontinuous method of separating neutral analytes that differ in hydrophobicity[90]. Briefly, a capillary is filled with a solution containing a charged detergent at a concentration higher than its critical micellar concentration. Analytes with different hydrophobicities can partition between free solution and the micelles at different rates (**Figure 5.1**). In an electric field, charged micelles begin to migrate and transport molecules with greater hydrophobicity across further distances, thus, spatially resolving them from less hydrophobic molecules. Both cationic and anionic micelles can be used in MEKC and selected for the appropriate target molecule. Furthermore, as most pharmaceuticals require enantiomer separations, chiral surfactants

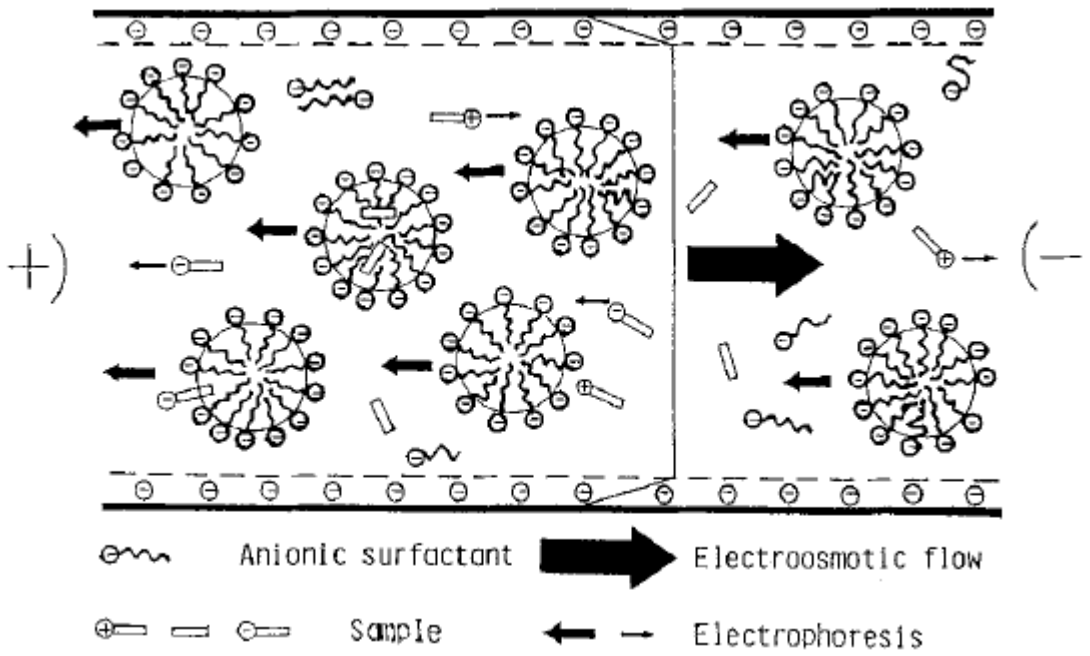

Figure 5.1: Schematic illustration of the separation principle of micellar EKC. Adapted from **Ref. 90** with permission from Wiley.

can also be added to enable separation. Though the principles of MEKC could easily be adapted to a FFE design, such a design has yet to be applied.

5.1.1.2 Dielectrophoresis

Neutral dipole species can be separated by dielectrophoresis, which is limited to large analytes (larger than nanometer in size). The theory of dielectrophoresis states that neutral particles can be resolved by a non-uniform electric field due to differences in dipole moments. A free-flow dielectrophoretic device was proposed[91], and recently implemented in the purification of tumour circulating cells[92]. The separation of smaller neutral molecules by dielectrophoresis, however, is challenging as small molecules have small dipole moments and require impractically high electric field gradients.

5.2 Non-Orthogonal-to-the-Flow Free-Flow Electrophoresis

Both MEKC and dielectrophoresis are well established purification techniques with their own respective niches, but can require complex experimental designs. The FFE modes that were previously described in **Chapter 1** can increase separation power as well. FFIZE can increase separation power by reducing the band broadening effects that are associated with hydrodynamic dispersion of a sample through the separation channel, and FFIEF can significantly increase resolution by the focussing effects. However, FFIZE provides separation only during discontinuous flow conditions, and FFIEF is only practical for the separation of ampholytes. There is another potentially viable method to increase the separation power of FFE, without the need to drastically modify the experimental setup. Again, I propose a geometric modification. Researchers in the Krylov group have demonstrated, from first principles, the possibility of increasing separation power by simply re-orientating the direction of the electric field with respect to the hydrodynamic flow[9193,94] (**Figure 5.2**). This new variation of FFZE is called Non-Orthogonal-to-the-Flow Electrophoresis (NOFFE). The next section describes the optimization of the direction of the electric field relative to the hydrodynamic flow in order to maximize the residence time of the sample within it. Moreover, I will present theoretic proof of the fact that a non-orthogonal field to the hydrodynamic flow offers better resolution between two species with comparable electrophoretic mobilities.

5.3 NOFFE Theory

FFE resolution (R_s), in general, can be defined as the following:

$$R_s = \frac{2\Delta x}{w_1 + w_2} \qquad (\mathbf{5.1})$$

where Δx is the distance between the centers of two different analyte streams, and w is the width of each analyte stream. In an updated equation, FFE resolution can be described as a function that is dependent on

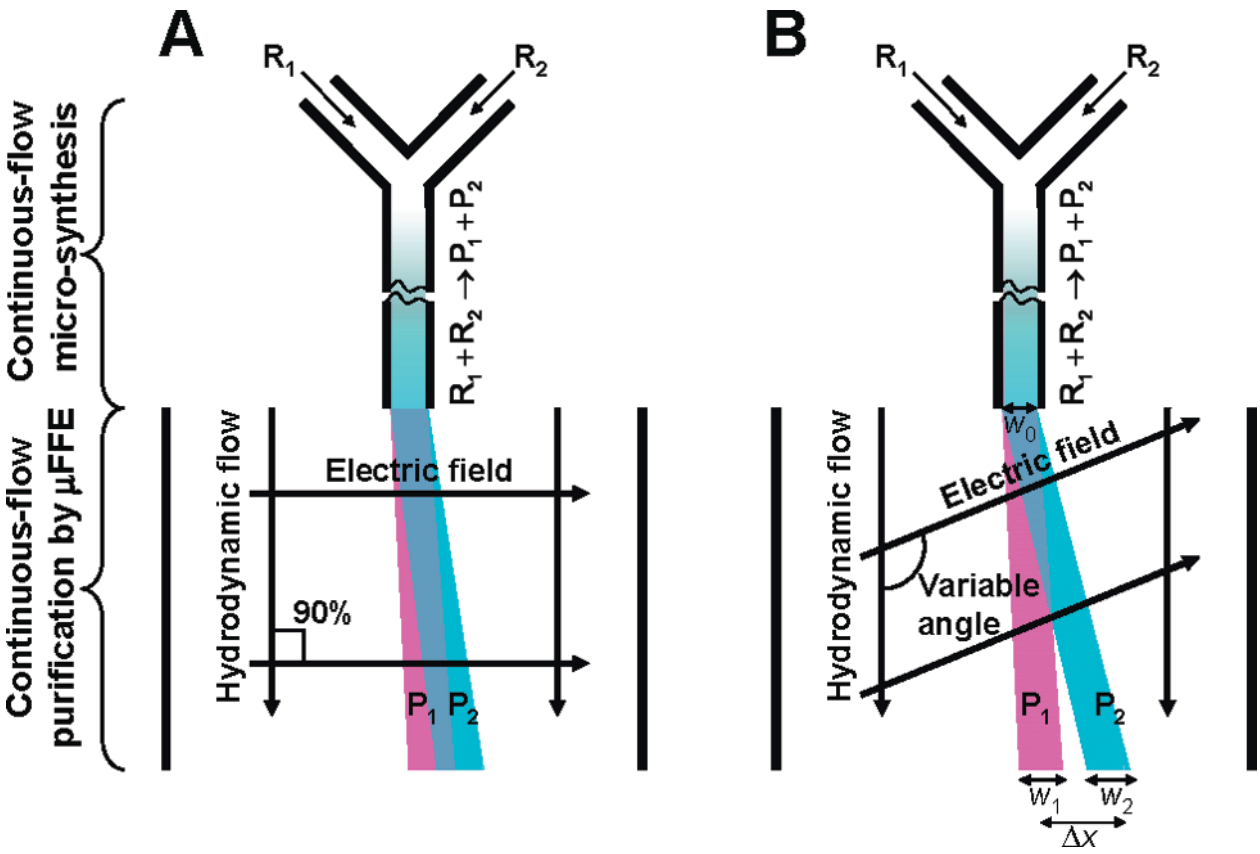

Figure 5.2: Schematic representation of separation of products P1 and P2 in an integrated system for in-flow microsynthesis followed by micropurification by µFFE with orthogonal (**A**) and nonorthogonal (**B**) orientations of the electric field and hydrodynamic flow. Reprinted with permission from Okhonin, V.; Evenhuis, C. J.; Krylov, S. N. Anal. Chem. 2010, 82, 1183. Copyright 2010 American Chemical Society

the angle at which the electric field is directed with respect to the hydrodynamic flow[91]. When a FFE device with an orthogonal electric field is used, the electromigration of the sample can only exist in a direction perpendicular to that of the hydrodynamic flow. Alternatively, when an electric field is directed non-orthogonal to the flow the elecromigration of the sample can be projected at an angle that directs it against (or with) the flow. In order to maximize separation, the species (with similar electrophoretic mobilities) should be directed against the flow to increase their residence time within the electric field. Species with larger electrophoretic velocities are delayed longer within the non-orthogonal electric field and experience larger lateral displacements than species with smaller electrophoretic velocities. As a result, the two species will migrate at appreciably different velocities, which allow them to separate.

Although band broadening is also increased, as a result of longer residence times, the widths of the analyte streams increase at a smaller rate than their lateral separation; overall resolution is improved. This fact is important because it explains why a device cannot simply be elongated to increase the residence time. Next, I will explain how this can be achieved theoretically.

Similar to all other modes of FFE, NOFFE requires a number of conditions to be met in order to maximize separation power. These conditions include temperature uniformity, optimal separation channel depth, and electroosmotic flow regulation. Temperature and channel depth are important in controlling band broadening, whereas electroosmotic flow is important in controlling the effective analyte velocity. Separation in FFE is achieved because different species migrate at unique velocities. Species exposed to an electric field in all modes of FFE, except NOFFE, will migrate with a velocity defined only by v_x (**Figure 5.3**). The novelty of NOFFE is that it introduces an electrophoretic velocity component, v_y, which contributes to the sample migration along the same axis as the hydrodynamic flow. v_y is highly dependent on the size of the species that is to be separated. Large or slowly diffusing molecules were calculated to have v_y that are similar to v_{hyd}, which is the velocity of the hydrodynamic flow, at any electric field angle.

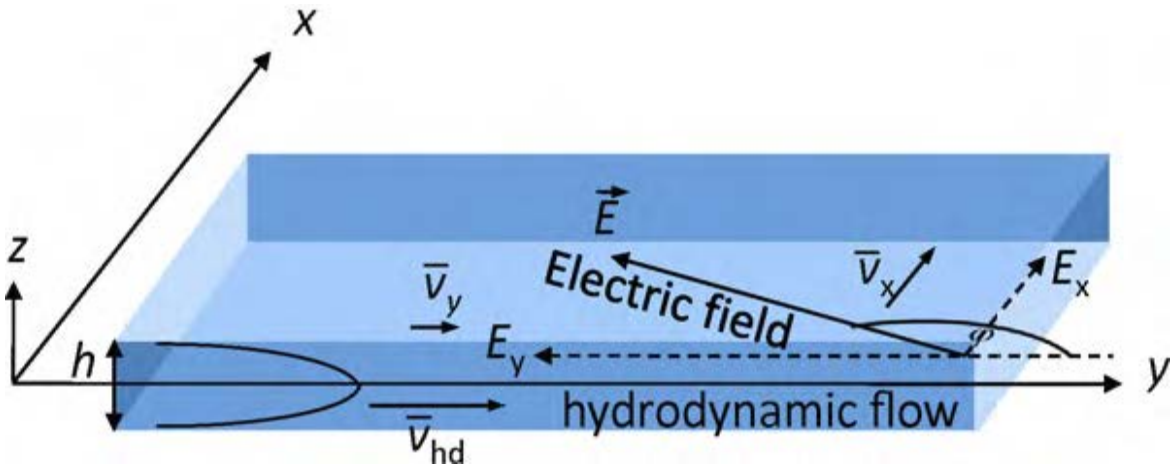

Figure 5.3: Schematic diagram defining the geometry on non-orthogonal FFE. The meanings of the symbols are as follows: v_{hd} is the average velocity of the hydrodynamic flow, v_x and v_y are components of the average resultant velocity of a species in the direction perpendicular and parallel to the hydrodynamic flow, respectively, E is the electric field strength with components E_x and E_y, and ϕ is the angle between the direction of the hydrodynamic flow and the electric field. Reproduced from **Ref. 94** with permission from Elsevier.

As a result, it can be difficult to increase the resolution between large species using NOFFE. Any increase in resolution is due to lateral separation being achieved faster than the effects of hydrodynamic dispersion as the electric field angle increases (**Figure 5.4A)**. In fact, diffusion and hydrodynamic dispersion are significantly reduced in the y-direction. The true potential of NOFFE, however, is observed when small molecules are exposed to a non-orthogonal field.

Smaller molecules show a significant increase in resolution as the electric field angle deviates orthogonally (**Figure 5.4B**). Lateral separation increases rapidly and, unlike the case with large molecules, follows exponential trends. Small species are more sensitive to slight changes in the electric

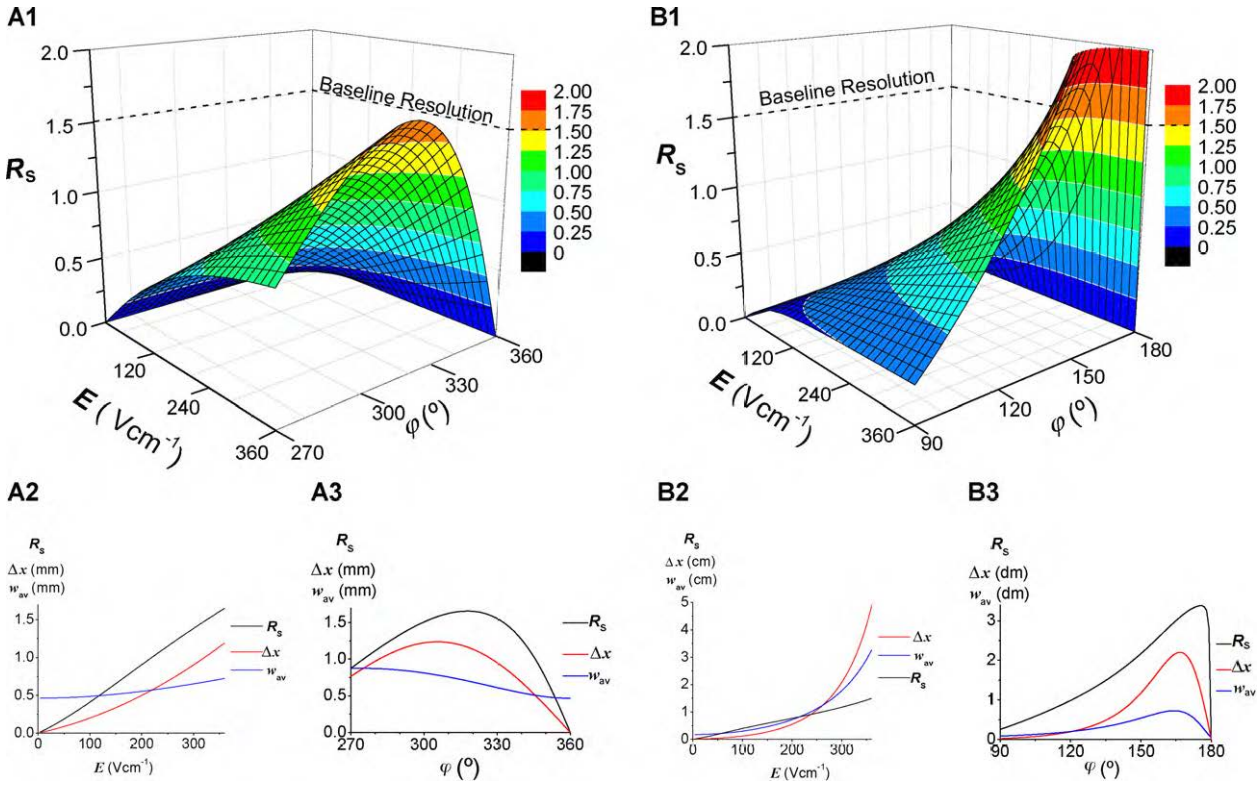

Figure 5.4: The variation of resolution, R_S, with electric field strength, E, and the angle, ϕ, between the electric field and the hydrodynamic flow, for: two large molecules (**A**) and two small molecules (**B**). The conditions used in all panels were: v_{hd} = 0.4 mm s^{-1}, h=20μm, and = 0.043 Sm^{-1}. In (**A1**–**A3**), μ_{EOF} = 1.80×10−8 $m^2s^{-1}V^{-1}$, and in (**B1**–**B3**), μ_{EOF} = −4.50×10−8 $m^2s^{-1}V^{-1}$. The vertical scale in **B1** has been truncated for clarity of presentation. Panels (**A2** and **B2**) depict the variation of resolution, separation, and average bandwidth with electric field strength for fixed ϕ values of 315° and 135°, respectively. Panels (**A3** and **B3**) show the variation of resolution, separation, and average stream width with ϕ for E=360 Vcm^{-1}. Reproduced from **Ref. 94** with permission from Elsevier.

field angle, and such a benefit is unprecedented for electrophoretic purifications. NOFFE can enable increased separation power of small molecules. For CFC integration, where a major goal is small molecule separation, NOFFE is a potentially viable solution for resolving small species with similar electrophoretic mobilities. Constructing NOFFE devices, however, will not be trivial. Having electrodes placed in the path of the hydrodynamic flow presents a number of challenges. For instance, solving the bubble problem and reducing pH gradients both depend greatly on the orientation of the electrodes. In NOFFE, bubbles will be capable of flowing with the hydrodynamic flow and into the separation channel, and may not be easily removed by either chimneys or SacCs. Flow, in general, will need to be modelled accurately to ensure flow uniformity. It is also likely that more steady-state issues can arise anew. In the next sections, I will outline the progress made so far in modelling and prototyping NOFFE devices.

5.4 *In silico* Optimization of NOFFE

Before attempting a real prototype, I modelled both the electric field and flow profiles of a virtual NOFFE device. The goal was to simulate virtual NOFFE devices having 3 different electrode configurations, which result in different electric field angles to the hydrodynamic flow: I chose electric field angles of 30°, 45°, and 60° to the electric field. Preliminary electric field and flow optimization, however, was attempted on the virtual device with an electric field angle of 45°. **Figure 5.5** and **Figure 5.6** illustrate the electric field and flow profiles, respectively, in the 45° NOFFE device. The electric field is demonstrated to be mostly uniform between electrodes. From the simulation, a sample should be exposed to the maximum electric field strength as long as the sample in injected below the top electrode and is not distorted by non-uniform flows. The hydrodynamic flow, however, is not uniform. This is expected since the electrode channels are non-orthogonal to the hydrodynamic flow. The first task was to model virtual variations in the NOFFE design that would not compromise flow uniformity.

5.4.1 Optimizing NOFFE Hydrodynamic Flow Profiles

Conventional FFE devices place the electrodes at the edges of the separation channel. In such devices, improving flow uniformity can be achieved by SacCs because they inhibit fluid exchange, as long as the hydrodynamic flow is parallel to the SacCs. A NOFFE device has electrodes placed directly in the path of the hydrodynamic flow, and this orientation prohibits the use of SacCs to improve flow uniformity; more channels would not improve the situation.

A major cause of flow non-uniformity in NOFFE designs is that the symmetry of a device is lost (**Figure 5.6**). If it is assumed that symmetry is vital for flow uniformity, then two additional channels that mirror the electrode channels will logically rectify any flow issues. I simulated the flow profile with these two extra channels, first in the 45° virtual device, and it was determined that re-introducing a symmetrical design can, indeed, prevent flow non-uniformity (**Figure 5.7A**). In fact, symmetrical designs can re-

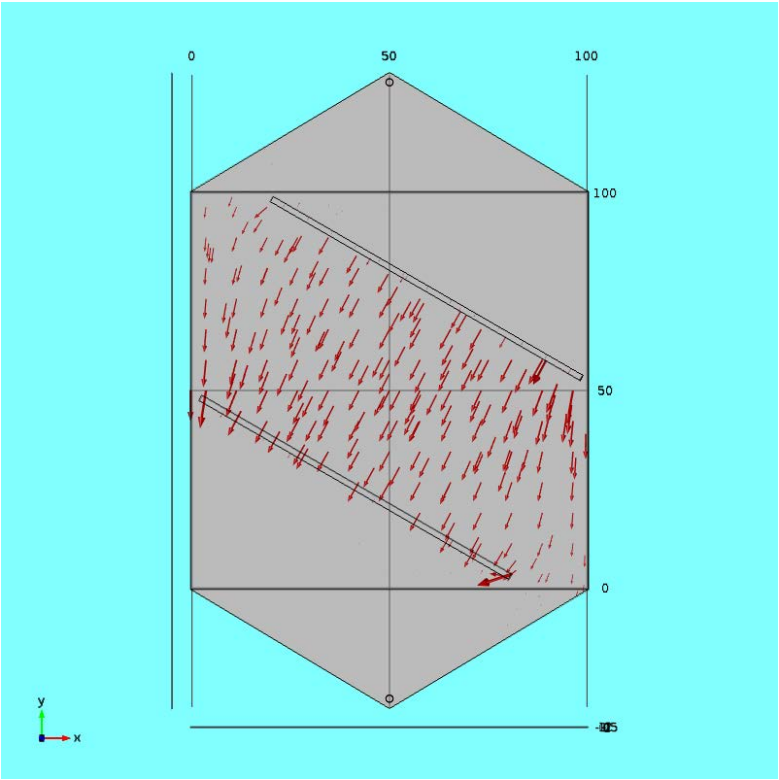

Figure 5.5: *In silico* simulation of the direction of the electric field in a NOFFE device, where the angle of the electric field is 45° to the hydrodynamic flow. The direction of the electric field is uniform between electrodes. Here the electric field strength is 100 V/cm.

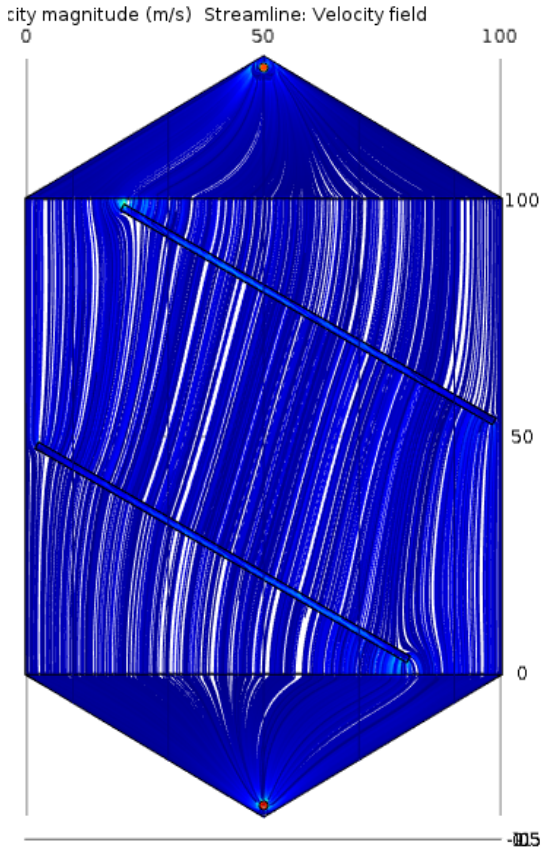

Figure 5.6: *In silico* simulation of the hydrodynamic flow profile in a NOFFE device where the electric field would be angled at 45° to the hydrodynamic flow. The flow is uniform between electrode channels; however the flow becomes non-uniform close to the ends of the deep channels. Such deviations may compromise separation quality. Here the hydrodynamic flow rate is 8 mL/min.

establish flow uniformity in all NOFEE designs (**Figure 5.7B,C**). The three symmetrical NOFFE designs, with 30°, 45°, and 60° electric field orientations, illustrate that the flow within each device approaches uniformity. Only in the NOFFE example with a 45° electric field angle, however, do the flow streamlines appear parallel. The other two devices may require further optimization. The present NOFFE designs, however, do not account for efficient bubble removal, as there are no chimneys. The addition of chimneys would likely need to be configured in symmetry. As in other FFE designs, however, chimneys would most likely compromise flow uniformity to a greater extent. Therefore, to simply future experiments chimneys cannot currently be used in conjunction with NOFFE and bubbles accumulation will have to be monitored

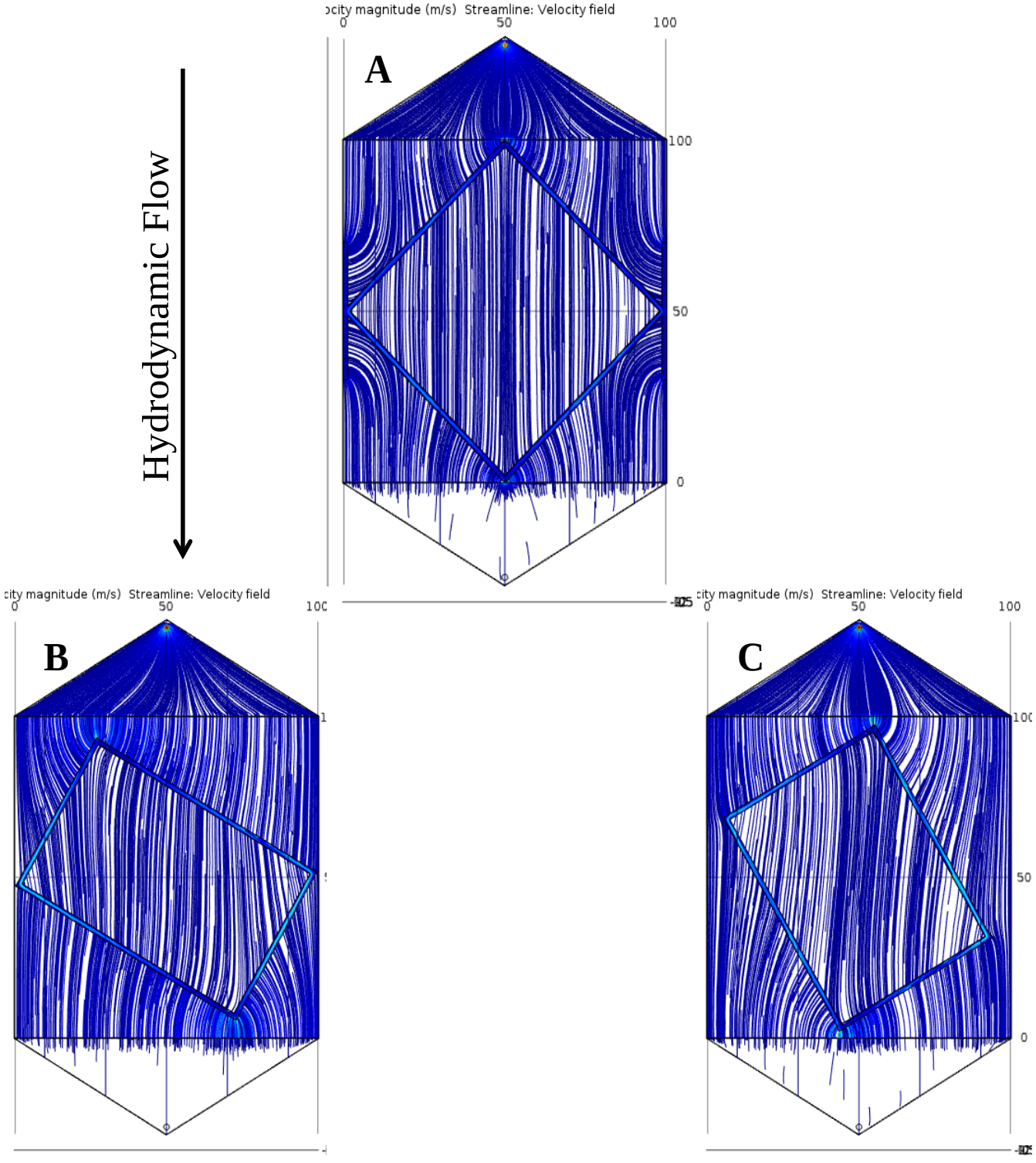

Figure 5.7: *In silico* modeling of flow profiles in three NOFFE virtual devices: (**A**) 45°; (**B**) 30°; and (**C**) 60°. In these simulations, flow streamlines are relatively uniform. Further optimization of the two latter designs may be necessary; however, this will be confirmed through future experiments. Here the flow rate is 8 mL/min

carefully. Presently, the goal of NOFFE is to demonstrate an increase in separation power, and the bubble problem can be addressed at a later time.

5.5 NOFFE Prototype

Multiple attempts to construct NOFFE prototypes have been successful. Milling is certainly the most efficient method of fabricating such devices because of the ability to prepare large aspect ratio channels in short periods of time. Devices were milled and assembled in less than 24 h. The prototypes were used successfully for the separation of rhodamine B and fluorescein, however, due to a saturation of bubbles within the separation channel the increase in resolution was inconclusive. Removing bubbles, by other means, may be necessary before advancing forward. The first experiments were performed at 50 – 100 V/cm, which are field strengths that are typically applied in mFFE. Reducing the electric field reduced bubble interference; however, it also provided poor resolving power that did not resolve the dyes sufficiently. At this stage in NOFEE development, new prototypes will require configurations to reduce bubble interference. More experiments are needed.

5.6 Conclusions

The theoretical groundwork for NOFFE has been provided. Now, it is a matter of experimentally validating the potential increase in separation power that a non-orthogonal electric field can provide. I have simulated the flow profiles in three separate *in silico* NOFFE models and have optimized flow uniformity by implementing symmetrical designs. Constructing NOFFE devices are not trivial, however, and will require solving steady-state issues, *de novo*, to demonstrate increased separation power. Theoretical simulations demonstrated that the increased separation power of NOFFE is better suited for the separation of small molecules, which can be beneficial as a complement to CFC.

5.7 Materials and Methods

5.7.1 NOFFE Fabrication

Fabricating NOFFE designs followed the same scheme, as any other FFE prototype, prescribed in **Chapter 2**.

5.7.2 COMSOL

Simulating flow within a NOFFE device, with COMSOL, follows the same procedure as described in **Chapter 3**. Again, the Laminar Flow Physics module was used. Modelling electric fields however uses Electrostatics module and the equations that describe the simulation is the following:

Charge Conservation:

$$E = -\nabla V \quad \textbf{(5.2)}$$

$$\nabla \cdot (\mathrm{D}) = \rho_r$$

Where **(5.3)**

$$\mathrm{D} = (\epsilon_0 \epsilon_r \mathrm{E})$$

Electric Potential Condition: **(5.4)**

$$V = V_0 \quad \textbf{(5.5)}$$

Ground Condition

$$V = 0 \quad \textbf{(5.6)}$$

Where E is the electric field, V is the voltage, D is the constitutive relation of relative permittivities ε_o and ε_r, which are the permittivities of a vacuum and the material used.

5.7.3 Reagents and Materials

All reagents were purchased from Sigma-Aldrich, unless otherwise stated. A 25 mM 4-(2-hydroxyethyl)-1-piperazine-ethanesulfonic acid (HEPES, 99.5% purity) buffer solution with Triton X-100 (0.01% [w/v]) was adjusted to pH 7 with 10 M NaOH and used in all experiments. The buffer mixture

was deoxygenated by overnight N_2 bubbling. A separate 10% EtOH solution was used as a primary wash solution to wet the surfaces of the mFFE devices. All solutions were prepared using deionized H_2O (EMD Millipore, Mississauga, Canada), the electrical resistivity of which was 18.2 MΩ•cm. The hydrodynamic flow of the buffer was driven by a continuous flow syringe pump system (New Era Pump System Inc., Farmingdale, NY, USA). The power source used was a high-voltage Electrophoresis Power Supply EPS 3501 XL (Amersham Pharmacia Biotech, New Jersey, USA).

5.7.4 NOFFE Operation

The buffer flow rate used was 8.00 ± 0.05 mL/min. The electric field strengths used ranged from 50 to 100 V/cm inside the separation channel. Experiments were carried out at room temperature. The NOFFE device was placed on top of metal blocks, which were in contact with ice packs, to prevent overheating. 10 fraction collection outlets were integrated at the end of the NOFFE prototype to receive purified product.

LIMITATIONS

The most significant limitation, to date, for existing FFE technology is that FFE separation is still best suited for molecules with large differences in their electrophoretic mobilities. With the exception of NOFFE, presently a theoretical platform only, it is impossible to separate species with similar electrophoretic mobilities. For such species, purification may be optimal using a different separation technique, most likely discontinuous. FFE is also inefficient at purifying organic molecules, due to solubility issues and the problem associated with generating similar electric fields using organic solvents. To date, the separation of organic species is best suited by liquid extraction or HPLC. The success of CFC will depend on the ability to separate a wide variety of molecules, however, there are a limited number of CFP options.

With respect to the integration of FFE with CFC, limitations associated with FFE are uncertain because mFFE has just recently been hypothesized as a complement to CFC. I reasoned that steady-state purification is the most important factor to realize FFE integration. In this dissertation the issues that deteriorate steady-state purification have been thoroughly addressed. Furthermore, new device geometries have been optimized to reduce or completely prevent their degrading effects. Although these solutions should be easily transferrable to different scales of FFE, they may not be reasonable solutions for analogues of FFE. SacCs and chimneys provide optimal operation under the assumption that a hydrodynamic flow exists, and that the electrodes are orientated parallel to the hydrodynamic flow. FFIZE would not benefit from either SacCs or chimneys because of the fact that the electric field is applied when the hydrodynamic flow is absent. NOFFE, as well, could suffer from similar non-steady state conditions because electrodes are non-parallel to the hydrodynamic flow. It is likely that any new designs will be met with similar challenges.

New designs should be optimized *in silico* before prototyping. The limitation associated with milling, however, is that the optimized virtual geometry may not be possible. Therefore, prototyping is

limited by the precision of a milling machine. A milling machine can only provide precision in the order of 100 microns. In some earlier experiments, it was impossible to achieve reproducible results when attempting channel dimensions that approached 100 microns. It might be prudent to consider other methods of prototyping or consider combining a variety of fabrication methods.

CONCLUDING REMARKS

CFC is an exciting approach to chemical processing. Although the history of CFS spans back into the nineteenth century with large-scale synthesis, small-scale chemistry is only recently exploiting the benefits associated with it. Continuous-flow reactors can synthesize a variety of products with higher percent yields and greater efficiency. Ideally, continuous-flow synthesis should be complemented by continuous-flow purification. Currently, however, there are a limited number of purification platforms that could complement CFS. Liquid extraction and FFE are the most viable options to streamline CFC. Liquid extraction is ideal for organic separations, whereas FFE is well suited for aqueous separations. Liquid extraction, however, cannot purify multiple components without complex experimental configurations, and contamination can be a significant challenge. On the other hand, FFE in its most basic configuration is a method that can efficiently purify multiple analytes from contaminants. Steady-state continuous-flow purification by FFE, however, is challenging to achieve and maintain for prolonged periods of time.

The future of integrating CFP with CFC lies in the success of steady-state continuous-flow purification. This dissertation has discussed many limitations associated with FFE, the focus of which is its inability to maintain steady-state purification at the current stage of development for small-scale devices. Joule heating and electrolysis are mainly responsible for the reduced operation time, as well as the deteriorating separation quality of midscale, milli-, and micro-FFE. Joule heating compromises separation by inducing intense band broadening effects. Electrolysis produces bubbles and generates significant pH gradients, both of which can degrade separation quality over time. These adverse conditions have been minimized in macroscale FFE technology by the use of membranes and stabilization methods, among other strategies. The strategies used for macroscale FFE, however, are neither easily transferable to other FFE scales, nor are they equally effective at such scales. Steady-state purification in small-scale FFE is still challenging.

Promising strategies have been recently developed to circumvent the effects caused by Joule heating and electrolysis. Joule heating can be dissipated effectively when channels with large aspect ratios are used. A number of midscale and microscale FFE devices have used re-circulated cooling liquids and thermoelectric cooling plates to help remove heat quickly. In my work, the use of ice packs was sufficient to minimize Joule heating. The goal of this dissertation, however, was to focus more on the electrolysis-mediated effects.

To suppress the effects associated with bubbles I developed a new FFE device, called OEFFE, in which the electrolyte above the electrodes is exposed to the atmosphere through tall chimneys. Manufacturing an optimized design required *in silico* modelling to simulate the flow profiles in OEFFE. COMSOL multiphysics software was essential in the development of OEFFE design concepts. To achieve flow uniformity, deep and narrow SacCs were implemented between the chimneys and the separation channel. With this design, all bubbles that are generated through electrolysis are effectively evacuated from the electrolyte and from the device without influencing separation performance. As a result, OEFFE was able to maintain steady-state purification for over a 12 h period. Next, it was important to realize steady-state purification over a broad range of separation conditions. A caveat is that the best separation conditions can generate pH gradients; typically when high electric field strengths and low hydrodynamic flow rates are used. Again, deep SacCs were instrumental in generating a uniform pH across the width of the separation channel. The high flow rates within the SacCs allowed both H^+ and OH^- to be rapidly evacuated before migrating into the separation channel. As a result, mFFE separation conditions were achieved at higher electric field strengths and lower hydrodynamic flow rates.

With an effective and optimized combination of these strategies, it is conceivable to have indefinitely long steady-state continuous-flow purification by all scales of FFE. With further advances in separation power and the ability to purify neutral samples, FFE could become more versatile and suitable

for practical combination with CFS. Where the past 150 years were devoted to industrial and continuous-flow synthesis, the near future may well be devoted to complete CFC integration

FUTURE PLANS

FFE continues to develop in both fundamentals and applications [95]. In the Krylov lab, alone, there are a number of projects that will further promote the integration of FFE with CFC processing. Here, I will present some of those projects.

1) Successful Completion and Implementation of NOFFE

NOFFE theory has been proved from first principles and simulated in order to facilitate prototyping of the first successful device. With the assistance of COMSOL simulation, it is possible to accurately model flows, electric fields, and sample trajectories. Sample trajectories can be simulated *in silico* using the Transport of Chemical Species module. Furthermore, it will be possible to model multiple physical processes simultaneously to evaluate the influence that a non-orthogonal electric field, heat generation, pH gradients, and hydrodynamic flow will have on a variety of analytes. It will be prudent to use COMSOL, before prototyping, in order to validate an optimal NOFFE design efficiently. A variety of electric field angles should be tested in order to determine maximum separation between two species with similar electrophoretic mobilities.

2) Practical Separations

The Krylov lab is formally a bio-analytical lab and FFE is a well-suited purification technique for biological samples. Indeed, the literature reflects hundreds of articles where FFE has been used for bio-analytical purposes. The OEFFE prototype was first used recently to attempt the separation of the MutS protein from DNA. The original cell lysate was heat-treated to denature non-target proteins, as MutS is heat-stable, and then passed through OEFFE for purification. With the help of Jiayin Bao, we used an acetic acid buffer at a pH between the pK_a of DNA and the pI of MutS (pH = 4.2) so to ensure that each species had an opposite charge. After purification, which was performed over 2 hours at 100 V/cm in a

steady state using OEFFE, collected fractions were tested for the presence of MutS using SDS page. The following figure illustrates the preliminary results.

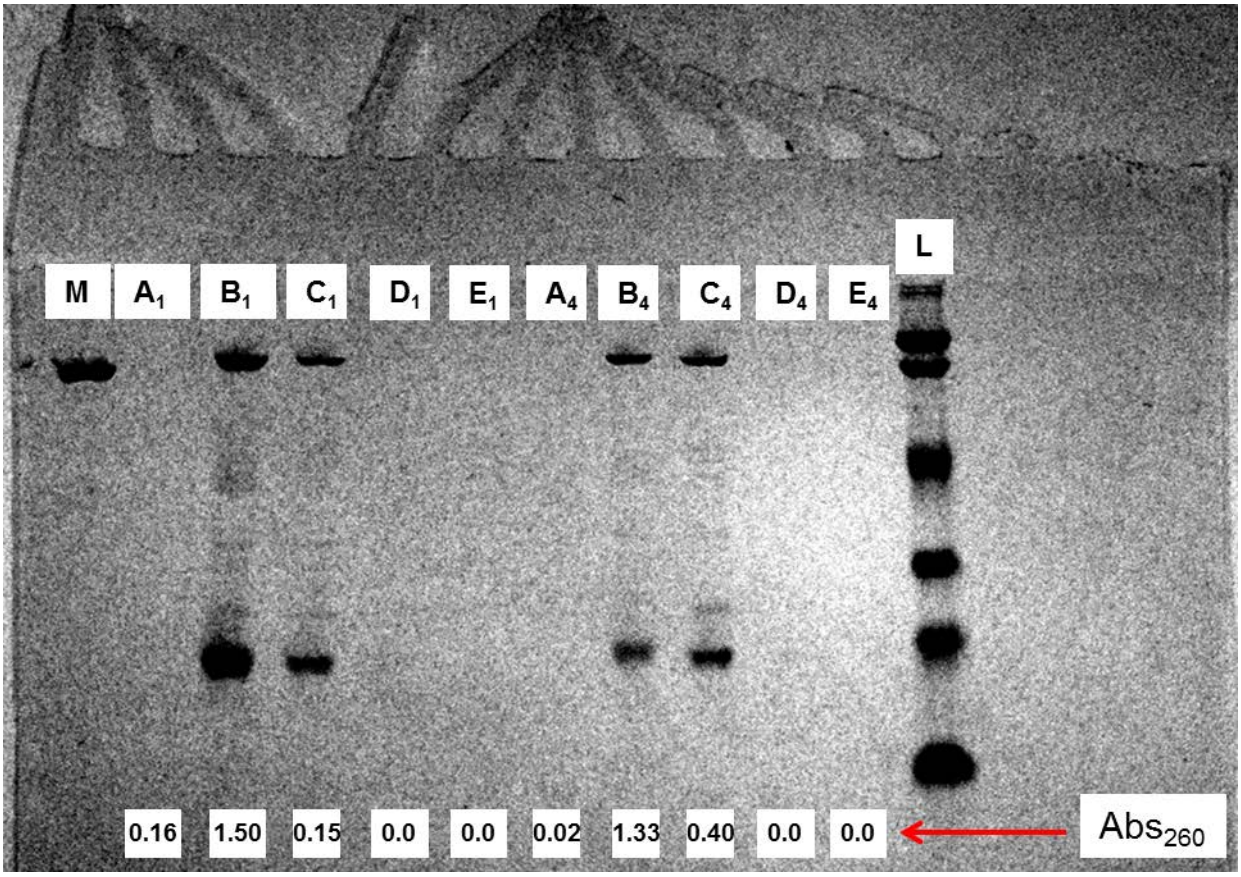

Figure S1: SDS page result of MutS separation from DNA using OEFFE. Lanes **A**-**E** represents the collection fractions with **A** and **E** being closest to the anode and cathode, respectively. The values below represent the relative absorbance value of DNA for each collection, and the values are only indicative of where DNA migrates. **M** represents pure MutS and **L** represents a molecular weight ladder. These results characterize the reproducible performance of OEFFE. The buffer was 10 mM acetic acid at pH 4.2, the electric field strength was 100 V/cm, the buffer flow was 8 mL/min and the sample flow rate was 10 µL/min.

DNA and MutS were not successfully resolved from each other; however, it is clear that both species did migrate under the experimental conditions. MutS was collected from two outlets, and DNA was observed in 3 outlets. With respect to the steady-state conditions, the migration of both DNA and MutS was consistent over 4 rounds of collection (2 hours). Such a separation, however, may be difficult because MutS is a DNA binding protein. Nevertheless, the intention was to use OEFFE for its first

practical separation. The results from the first test will give promising ideas on how to further optimize the new designs and configurations (i.e. an open electrolyte concept for FFIEF).

3) On-line detection and full CFC integration

In optimizing mFFE and OEFFE, visible concentrations of dyes were used to assist in the assessment of separation quality. There was no need for an elaborate detection system. Obviously, this is not ideal for practical separations. For the detection of MutS and DNA, off-line techniques were used. To successfully implement FFE with CFC, however, it will be necessary to develop a prototype that can integrate online detection. Conceivably, optical detection would be the easiest method of on-line detection in order to monitor the separation quality in real time. In the Krylov lab, we have expertise in spectroscopic techniques. In particular, we would have potential access to UV absorbance, fluorescence, and refractive index detection integrated with a FFE device. Each device would require separate configurations, and we are currently examining possible ways to develop them. The end goal would likely have MS integrated in-line with FFE. Such a design would allow 'sampling' at certain times and at specific locations in the separation channel, and these sample volumes would then be analysed by MS to monitor separation quality in real time. Although the benefits associated with MS detection are numerous compared with optical detection, integrating it with FFE will be significantly more challenging.

LIST OF PUBLICATIONS AND PATENTS

F. J. Agostino, L. T. Cherney, M. Kanoatov, and S. N. Krylov (2014), "Reducing pH Gradients in mFFE", *Analytical Chemistry,* 86 (12), 5656–5660.

F. J. Agostino, L. T. Cherney, V. Galievsky, and S. N. Krylov (2013). "Steady-State Continuous-Flow Purification by Electrophoresis", *Angewandte Chemie International Edition*, 52, 7256 –7260.

F. J. Agostino, C. J. Evenhuis, and S. N. Krylov (2011). "Milli Free-Flow electrophoresis: I. Fast Prototyping of mFFE devices", *Journal of Separation Science*, 34, 556-564.

F. J. Agostino, and S. N. Krylov (2013). "Free-Flow Electrophoresis Device and Method", *U.S. Provisional Patent (61/829,841).*

REFERENCES

(1) Yoshida, J.-i.; Takahashi, Y.; Nagaki, A. *Chem. Commun.* **2013**, *49*, 9896.
(2) Aftalion, F. *A History of the International Chemical Industry*; University of Pennsylvania Press: Philadelphia, 1991.
(3) Anastas, P. T.; Warner, J. *Green Chemistry Theory and Practice*; Oxford University Press: Oxford, 1998.
(4) Poliakoff, M.; Fitzpatrick, J. M.; Farren, T. R.; Anastas, P. T. *Science* **2002**, *297*, 807.
(5) Clark, M. A.; Acharya, R. A.; Arico-Muendel, C. C.; Belyanskaya, S. L.; Benjamin, D. R.; Carlson, N. R.; Centrella, P. A.; Chiu, C. H.; Creaser, S. P.; Cuozzo, J. W.; Davie, C. P.; Ding, Y.; Franklin, G. J.; Franzen, K. D.; Gefter, M. L.; Hale, S. P.; Hansen, N. J. V.; Israel, D. I.; Jiang, J.; Kavarana, M. J.; Kelley, M. S.; Kollmann, C. S.; Li, F.; Lind, K.; Mataruse, S.; Medeiros, P. F.; Messer, J. A.; Myers, P.; O'Keefe, H.; Oliff, M. C.; Rise, C. E.; Satz, A. L.; Skinner, S. R.; Svendsen, J. L.; Tang, L.; van Vloten, K.; Wagner, R. W.; Yao, G.; Zhao, B.; Morgan, B. A. *Nat. Chem. Biol.* **2009**, *5*, 647.
(6) Song, H.; Tice, J. D.; Ismagilov, R. F. *Angew. Chem. Int. Ed.* **2003**, *42*, 768.
(7) Jovanovic, J.; Rebrov, E. V.; Nijhuis, T. A.; Hessel, V.; Schouten, J. C. *Ind. Eng. Chem. Res.* **2010**, *49*, 2681.
(8) Sauks, J. M.; Mallik, D.; Lawryshyn, Y.; Bender, T. P.; Organ, M. G. *Org. Process Res. Dev.* **2014**, *18*, 1310.
(9) Moore, J. S.; Jensen, K. F. *Org. Process Res. Dev.* **2012**, *16*, 1409.
(10) Malet-Sanz, L.; Susanne, F. *J. Med. Chem.* **2012**, *55*, 4062.
(11) Hartman, R. L.; McMullen, J. P.; Jensen, K. F. *Angew. Chem. Int. Ed.* **2011**, *50*, 7502.
(12) Mastronardi, F.; Gutmann, B.; Kappe, C. O. *Org. Lett.* **2013**, *15*, 5590.
(13) Wiles, C.; Watts, P.; Haswell, S. J.; Pombo-Villar, E. *Tetrahedron* **2005**, *61*, 10757.
(14) Ullah, F.; Samarakoon, T.; Rolfe, A.; Kurtz, R. D.; Hanson, P. R.; Organ, M. G. *Chem. – Eur. J.* **2010**, *16*, 10959.
(15) Reichart, B.; Tekautz, G.; Kappe, C. O. *Org. Process Res. Dev.* **2013**, *17*, 152.
(16) Roth, G. P.; Stalder, R.; Long, T. R.; Sauer, D. R.; Djuric, S. W. *J. Flow Chem.* **2013**, *3*, 34.
(17) Carroccia, L.; Musio, B.; Degennaro, L.; Romanazzi, G.; Luisi, R. *J. Flow Chem.* **2013**, *3*, 29.
(18) Rajendran, A.; Paredes, G.; Mazzotti, M. *J. Chromatogr. A* **2009**, *1216*, 709.
(19) Kessler, L. C.; Seidel-Morgenstern, A. *J. Chromatogr. A* **2006**, *1126*, 323.
(20) Hur, J. S.; Wankat, P. C. *Ind. Eng. Chem. Res.* **2006**, *45*, 8713.
(21) Minceva, M.; Gomes, P. S.; Meshko, V.; Rodrigues, A. E. *Chem. Eng. J.* **2008**, *140*, 305.
(22) Wojik, A.; Marr, R. *Chem. Ing. Tech.* **2005**, *77*, 653.
(23) Benz, K.; Jackel, K.-P.; Regenauer, K.-J.; Schiewe, J.; Drese, K.; Ehrfeld, W.; Hessel, V.; Lowe, H. *Chem. Eng. Technol.* **2001**, *24*, 11.
(24) Kralj, J. G.; Schmidt, M. A.; Jensen, K. F. *Lab Chip* **2005**, *5*, 531.
(25) Kralj, J. G.; Sahoo, H. R.; Jensen, K. F. *Lab Chip* **2007**, *7*, 256.
(26) Heider, P. L.; Born, S. C.; Basak, S.; Benyahia, B.; Lakerveld, R.; Zhang, H.; Hogan, R.; Buchbinder, L.; Wolfe, A.; Mascia, S.; Evans, J. M. B.; Jamison, T. F.; Jensen, K. F. *Org. Process Res. Dev.* **2014**, *18*, 402.

(27) Campos, C. D. M.; Park, J. K.; Neuzil, P.; da Silva, J. A. F.; Manz, A. *RSC Adv.* **2014**, *4*, 49485.
(28) Freire, M. G.; Neves, C. M. S. S.; Marrucho, I. M.; Canongia Lopes, J. N.; Rebelo, L. P. N.; Coutinho, J. A. P. *Green Chem.* **2010**, *12*, 1715.
(29) Schuur, B.; Hallett, A. J.; Winkelman, J. G. M.; de Vries, J. G.; Heeres, H. J. *Org. Process Res. Dev.* **2009**, *13*, 911.
(30) Assmann, N.; Ladosz, A.; Rudolf von Rohr, P. *Chem. Eng. Technol.* **2013**, *36*, 921.
(31) Kim, S.; Han, S.-I.; Park, M.-J.; Jeon, C.-W.; Joo, Y.-D.; Choi, I.-H.; Han, K.-H. *Anal. Chem.* **2013**, *85*, 2779.
(32) Mizuno, M.; Yamada, M.; Mitamura, R.; Ike, K.; Toyama, K.; Seki, M. *Anal. Chem.* **2013**, *85*, 7666.
(33) Strohmeier, O.; Emperle, A.; Roth, G.; Mark, D.; Zengerle, R.; von Stetten, F. *Lab Chip* **2013**, *13*, 146.
(34) Toh, P. Y.; Yeap, S. P.; Kong, L. P.; Ng, B. W.; Chan, D. J. C.; Ahmad, A. L.; Lim, J. K. *Chem. Eng. J.* **2012**, *211-212*, 22.
(35) Caparros, C.; Benelmekki, M.; Martins, P. M.; Xuriguera, E.; Silva, C. J. R.; Martinez, L. M.; Lanceros-Mendez, S. *Mater. Chem. Phys.* **2012**, *135*, 510.
(36) Kang, J. H.; Park, J.-K. *Small* **2007**, *3*, 1784.
(37) Hannig, K.; Wirth, H.; Meyer, B.-H.; Zeiller, K. *H.-S. Z. Physiol. Chem.* **1975**, 1209.
(38) Hannig, K.; Wirth, H.; Schindler, R. K.; Spiegel, K. *H.-S. Z. Physiol. Chem.* **1977**, *358*, 753.
(39) Agostino, F. J.; Evenhuis, C. J.; Krylov, S. N. *J. Sep. Sci.* **2011**, *34*, 556.
(40) Raymond, D. E.; Manz, A.; Widmer, H. M. *Anal. Chem.* **1994**, *66*, 2858.
(41) Agostino, F. J.; Cherney, L. T.; Kanoatov, M.; Krylov, S. N. *Anal. Chem.* **2014**, *86*, 5656.
(42) Kohler, S.; Weilbeer, C.; Howitz, S.; Becker, H.; Beushausen, V.; Belder, D. *Lab Chip* **2011**, *11*, 309.
(43) Kohlheyer, D.; Eijkel, J. C. T.; van den Berg, A.; Schasfoort, R. B. M. *Electrophoresis* **2008**, *29*, 977.
(44) Bauer, J.; Weber, G. *J. Disper. Sci. Technol.* **1998**, *19*, 937.
(45) Justesen, B. H.; Laursen, T.; Weber, G.; Fuglsang, A. T.; Moeller, B. L.; Gunther Pomorski, T. *Anal. Chem.* **2013**, *85*, 3497.
(46) Shao, J.; Fan, L.-Y.; Cao, C.-X.; Huang, X.-Q.; Xu, Y.-Q. *Electrophoresis* **2012**, *33*, 2065.
(47) Weber, G.; Bocek, P. *Electrophoresis* **1996**, *17*, 1906.
(48) McMullen, J. P.; Jensen, K. F. *Annu. Rev. Anal. Chem.* **2010**, *3*, 19.
(49) Comer, E.; Organ, M. G. *J. Am. Chem. Soc.* **2005**, *127*, 8160.
(50) Schenk, R.; Hessel, V.; Hofmann, C.; Kiss, J.; Löwe, H.; Ziogas, A. *Chem. Eng. J.* **2004**, *101*, 421.
(51) Wiles, C.; Watts, P. *Eur. J. Org. Chem.* **2008**, 1655.
(52) Belder, D.; Nagl, S.; Tehsmer, V.; Jezierski, S. *Chem. Commun.* **2013**, *49*, 11644.
(53) Kockmann, N.; Roberge, D. M. *Chem. Eng. Technol.* **2009**, *32*, 1682.
(54) Tricotet, T.; O'Shea, D. *Chem-Eur. J.* **2010**, *16*, 6678.
(55) Rosenfeld, C.; Serra, C.; Brochon, C.; Hadziioannou, G. *Lab Chip* **2008**, *8*, 1682.
(56) Baumann, M.; Baxendale, I. R.; Martin, L. J.; Ley, S. V. *Tetrahedron* **2009**, *65*, 6611.

(57) Greener, J.; Li, W.; Ren, J.; Voicu, D.; Pakharenko, V.; Tangb, T.; Kumacheva, E. *Lab Chip* **2010**, *10*, 522.
(58) Shiu, P. P.; Knopf, G. K.; Ostojic, M.; Nikumb, S. *J. Micromech. Microeng.* **2008**, *18*, 025012.
(59) Mei, Q.; Xia, Z.; Xu, F.; Soper, S. A.; Fan, Z. H. *Anal. Chem.* **2008**, *80*, 6045.
(60) Rodrigues, E. R. G. O.; Lapa, R. A. S. *Microchim. Acta* **2009**, *166*, 189.
(61) Rodrigues, E. R. G. O.; Lapa, R. A. S. *Anal. Sci.* **2009**, *25*, 443.
(62) Sun, Y.; Kwok, Y. C.; Nguyen, N.-T. *J. Micromech. Microeng.* **2006**, *16*, 1681.
(63) Zhu, X.; Liu, G.; Guo, Y.; Tian, Y. *Microsyst. Technol.* **2007**, *13*, 403.
(64) Fonslow, B. R.; Barocas, V. H.; Bowser, M. T. *Anal. Chem.* **2006**, *78*, 5369.
(65) Raymond, D. E.; Manz, A.; Widmer, H. M. *Anal. Chem.* **1996**, *68*, 2515.
(66) Kohlheyer, D.; Eijkel, J. C. T.; Schlautmann, S.; van den Berg, A.; Schasfoort, R. B. M. *Anal. Chem.* **2008**, *80*, 4111.
(67) Fonslow, B. R.; Bowser, M. T. *Anal. Chem.* **2008**, *80*, 3182.
(68) Persat, A.; Suss, M. E.; Santiago, J. G. *Lab Chip* **2009**, *9*, 2454.
(69) Revermann, T.; Gotz, S.; Kunnemeyer, J.; Karst, U. *Analyst* **2008**, *133*, 167.
(70) Vogt, H. *J. App. Electrochem.* **1983**, *13*, 87.
(71) Turgeon, R.; Bowser, M. *Anal. Bioanal. Chem.* **2009**, *394*, 187.
(72) Frost, N.; Bowser, M. *Lab Chip* **2010**, *10*, 1231.
(73) Terabe, S. *J Pharm Biomed Anal* **1992**, *10*, 705.
(74) Terabe, S.; Otsuka, K.; Ando, T. *Anal. Chem.* **1985**, *57*, 834.
(75) Rizvi, S. A. A.; Do, D. P.; Saleh, A. M. *Eur. J. Chem.* **2011**, *2*, 276.
(76) Gascoyne, P. R. C.; Vykoukal, J. *Electrophoresis* **2002**, *23*, 1973.
(77) Hughes, M. P. *Electrophoresis* **2002**, *23*, 2569.
(78) Millioni, R.; Franchin, C.; Tessari, P.; Polati, R.; Cecconi, D.; Arrigoni, G. *J. Chromatogr. A* **2013**, *1293*, 1.
(79) Heydt, A.; Mosher, R. A. *Electrophoresis* **1989**, *10*, 697.
(80) Kohlheyer, D.; Besselink, G. A. J.; Schlautmann, S.; Schasfoort, R. B. M. *Lab Chip* **2006**, *6*, 374.
(81) Yin, X.-Y.; Dong, J.-Y.; Wang, H.-Y.; Li, S.; Fan, L.-Y.; Cao, C.-X. *Electrophoresis* **2013**, *34*, 2185.
(82) Jezierski, S.; Belder, D.; Nagl, S. *Chem. Commun.* **2013**, *49*, 904.
(83) Duso, A. B.; Chen, D. D. Y. *Anal. Chem.* **2002**, *74*, 2938.
(84) Agostino, F. J.; Cherney, L. T.; Galievsky, V.; Krylov, S. N. *Angew. Chem., Int. Ed.* **2013**, *52*, 7256.
(85) Yang, J.-H.; Shao, J.; Wang, H.-Y.; Dong, J.-Y.; Fan, L.-Y.; Cao, C.-X.; Xu, Y.-Q. *Electrophoresis* **2012**, *33*, 2925.
(86) Kumar, V.; Nigam, K. D. P. *Green Process. Synth.* **2012**, *1*, 79.
(87) Javaid, R.; Kawanami, H.; Chatterjee, M.; Ishizaka, T.; Suzuki, A.; Suzuki, T. M. *Chem. Eng. J.* **2011**, *167*, 431.
(88) Dubois, P.; Marchand, G.; Fouillet, Y.; Berthier, J.; Douki, T.; Hassine, F.; Gmouh, S.; Vaultier, M. *Anal. Chem.* **2006**, *78*, 4909.
(89) Fukuyama, T.; Rahman, M. T.; Sumino, Y.; Ryu, I. *Synlett* **2012**, *23*, 2279.
(90) Nishi, H.; Terabe, S. *Electrophoresis* **1990**, *11*, 691.

(91) Kirchoff, R. H.; Hamdi, A. *J. Electrochem. Soc.* **1973**, *120*, 80.
(92) Shim, S.; Stemke-Hale, K.; Tsimberidou, A. M.; Noshari, J.; Anderson, T. E.; Gascoyne, P. R. C. *Biomicrofluidics* **2013**, *7*, 011807/1.
(93) Okhonin, V.; Evenhuis, C. J.; Krylov, S. N. *Anal. Chem.* **2010**, *82*, 1183.
(94) Evenhuis, C. J.; Okhonin, V.; Krylov, S. N. *Anal. Chim. Acta* **2010**, *674*, 102.
(95) Kašička, V. *Electrophoresis* **2009**, *30*, S40.